Marine Performance Evaluation of a Fast Rescue Craft

by

© *Trevor Harris*, P. Eng.

A thesis submitted to the

School of Graduate Studies

in partial fulfilment of the

requirements for the degree of

Master of Engineering

Department of Engineering

Memorial University of Newfoundland

May 2018

St. John's Newfoundland & Labrador

Abstract

Marine performance evaluation was carried out aboard a fast rescue craft utilized by the Canadian Coast Guard. The experiments were conducted in late 2016 in the waters off Conception Bay South, NL and St. John's, NL. The three primary focus areas of the study were vessel performance, fuel economy, and human kinetics.

The evaluated vessel has a unique propulsion arrangement and is the first to be outfitted in Canada with Mercury Marine DSI 3.0 spark-ignited diesel outboard motors. Motivations to use this type of engine are to unify the Coast Guard's fuel supply and to also allow engine re-start after inversion. The Canadian Coast Guard is interested in this vessel's performance in comparison to the rest of the fleet because of these intrinsic advantages.

The performance tests concluded that the vessel is very reactive to helm input. It also has much greater directional stability as its speed increases. It can reach its maximum speed in 250 metres, taking approximately 20 seconds to do so. At a full speed of 38 knots, the vessel can execute a 180^{o} turn in just over 200 metres, and just under 20 metres at manoeuvring speed. The vessel can also tow a 19.7 metre fishing vessel at speeds up to 4.5 knots.

The trials showed that the fuel economy was not overly sensitive to wind speed, wind direction, or even wave height. The fuel consumption curve fits a resistance curve that is typical of a planing craft. Its maximum range of 56 nautical miles is achieved at its optimal cruising speed of 24.6 knots.

The vessel motions show that the accelerations in the Z direction are the most prominent. The accelerations in the X direction are the lowest, with accelerations in

the Y directions being slightly higher. The maximum observed Z acceleration was 4.76 times gravity. The helmsman's ability to maintain heading is increased with speed due to the higher directional stability observed at higher speeds. Wave height also has a prominent effect on the helmsman's ability to maintain heading.

Acknowledgements

I must first and foremost attempt to thank my wife, Nadine, for her encouragement and support. I say attempt since her patience and understanding over the past few years cannot be recognized with mere paper and ink. I can only guess at the number of questions that went unanswered as I stared at my computer screen, completely unaware of my surroundings; I will attempt to repay her with more attention in the future.

I would like to thank my thesis adviser, Dr. Dan Walker, for his mentoring over the last decade; his faith in me predates this thesis by many years. I started out as a student of Dr. Walker and then worked as his employee for six years; his support has not wavered throughout.

I would also like to thank the experts at the National Research Council for their persistent efforts with this project. I must express my gratitude to Matthew Garvin and Derek Butler who have been absolute key members in the planning and execution of this project. Many hard hours have been undertaken by both, leading to the invaluable data collected and presented herein.

This effort was heavily supported by the Canadian Coast Guard crew involved with this project: Neil Peet, Glen Saunders, Brian Pye, and Steve Sheppard. Their expertise allowed this challenging project to be executed to the highest standard.

Finally, I'd like to thank my cat, Willow, for continually walking over my computer keyboard to give me love. Her actions in this regard have necessitated I scour this thesis to ensure not one word is order out of.

Contents

List of Tables

List of Figures

Chapter 1

Introduction

The Canadian Coast Guard (CCG) has recently procured a new type of fast rescue craft (FRC). Marine performance evaluation was carried out on this vessel focusing on the areas of vessel performance, fuel economy, and human kinetics.

The craft utilized for the study was *CG 289*. The primary motivation for the choice of this vessel was its propulsion arrangement. This vessel is the first to be outfitted in Canada with Mercury Marine DSI 3.0 spark-ignited diesel outboard motors. These engines are a new innovation from Mercury Marine that utilize diesel as the fuel supply as opposed to gasoline. Provisions are made to ensure the historically heavy engine block of a diesel engine is made sufficiently light to be packaged in an outboard configuration [1].

The CCG is interested in this propulsion arrangement for quite a number of reasons. The first motivation is to streamline its fuel supply to a uniform hydrocarbon; should the fuel which runs their large ships also be used to supply their FRC's (which run on significantly less fuel), then this would yield a nearly infinite supply for the

FRC. Also, shore-based fuelling stations such as marinas and fish plants are more readily equipped to supply diesel fuel than gasoline. This allows FRC's to be supported by numerous shore based fuelling stations rather than relying on large vessel support. Secondly, diesel engines are more tolerant to physical inversion than gasoline engines. This FRC is equipped with self-righting equipment in the event of accidental capsizing, but without the ability to start the engines after an event, the vessel would still be disabled. Finally, carrying gasoline is a shipboard fire hazard since it is much more volatile compared to diesel.

The FRC was outfitted with a variety of data acquisition and monitoring equipment. At sea experiments, similar to sea trials, were conducted in late 2016 in the waters off Conception Bay South and St. John's, NL. Additionally, the data acquisition equipment remained on board between experiment days and acquired the FRC's daily use, which added to the cloud of data available to be analysed.

The collected data was analyzed using an object-oriented codebase inside the Matlab© software environment. Each type of experiment conducted was analyzed in its own way with its own individual requirements, however, all collected data was used to populate the performance curves.

This thesis describes the vessel, data acquisition setup, experiments performed, analysis methods, results, and conclusions of the work.

Chapter 2

Literature Review

Much work has been completed in the evaluation of planing hulls through numerical simulation, scaled model experiments, and full scale evaluation. Work relevant to this thesis is reviewed below. The issues of hull performance in calm water and waves are explored as well as relevant experimental methods. A number of data mining papers in this area are discussed as well.

2.1 Fridsma (1969)

In 1969, a model experimental program was undertaken for a variety of hull forms to determine calm and rough water performance of planing hulls [2]. The experiments took place in the Davidson Laboratory at the Stevens Institute of Technology. Motions and accelerations in heave and pitch were measured for a variety of speeds. It was noted that the vessels motions increased nearly linearly with speed and wave to a certain point. It was found at higher speeds (approximately 25-30 knots), however, this effect seems to level off on a second order type curve. This has been corroborated

with the experience felt by the operators who describe the vessels as feeling "stiffer" at higher speeds. The accelerations follow a similar trend, but the extent of the linear relationship extends further into the speed range than appears to be the case with the motions. The experiments conducted within this thesis are to be performed at a variety of speeds. Particular attention will be adhered to whether or not this phenomena is perceived.

2.2 Blount and Codega (1992)

In an attempt to gather more information on the previous, a paper was reviewed that gave insight to stability at high speeds. Dynamic stability was explored by Blount and Codega (1992) from a designer's perspective [3]. The authors conclude that various dynamic instabilities in the form of bow steering, chine riding, and porpoising are heavily dependant on speed and location of longitudinal centre of gravity. Additionally, they showed that ventilation of the propellers in a transverse or combined seaway will induce roll moments and cause asymmetrical heel angles leading to undesirable running attitudes. These dynamic instabilities are different than Fridsma had uncovered in that while the vessel may seem stiffer to manouver, it is less stable at higher speeds. It was hoped that the experiments conducted in this thesis would add clarity to these notions.

2.3 Brown and Klosinki (1994)

A paper in the area of directional stability was studied by Brown and Klosinki (1994), also at Stevens Institute of Technology's Davidson Laboratory. This was completed through the use of captive model tests [4]. In this experiment, two hulls of different deadrise angles of 10° and 20° were tested. Three trim angles were studies for each: 0°, 3°, and 6°. It was observed that at 0°, the roll stiffness decreased with speed. However, at 3°, the roll stiffness increased with speed nearly linearly, and takes the form of a second order polynomial with the 6° trim case. This study is more inlign with the findings of Fridsma (1969).

2.4 Payne (1994)

As fuel consumption is directionally proportional to resistance, a compilation paper of various resistance studies was explored. Payne (1994) compiled data from a number of towing tank experiments comparing resistance curves to empirical equations [5]. His method employed a modified added mass portion of the equations yielding just 3% error with the towing experiments. Payne's work suggests that above a certain speed, the buoyancy is zero when the wetted length is less than the beam. This may suggest that the increase in directional stability is due to the inward resolved hydrodynamic forces at higher speeds. The results within this thesis are comparable with the results of Payne (1994).

2.5 MacPherson (2003)

Several papers were reviewed to gain insight into execution and standards for full scale planing craft trials. MacPherson (2003) published a paper on the value of sea trial data [6]. This effort outlined a simplistic sea trial program with minimal data acquisition instrumentation performed on a 49 foot long work boat. The purpose of the experiment was to evaluate an under-performing planing vessel. The results of the experiment proved gearing ratio and propeller selection not only limited the speed, but also simultaneously increased the fuel consumption of the vessel. The data presented in the work shows benchmarks that can be used in comparison of the results within this thesis.

2.6 Mennen, Van den Boom, and Verkyl (2006)

In 2006, Mennen et al. reviewed the current standards for performance and analysis of speed trials as part of a Joint Industry Project (JIP) led by the Maritime Research Institute Netherlands (MARIN) [7]. Together with ship owners they compiled a recommended practise for conducting trials including required data acquisition, procedures, and contents of reporting. The report outlines standards and tolerances of various measurements for compliance. These standards were used as a minimum baseline when designing the data acquisition system, test execution, and analysis of the work contained within this thesis.

2.7 Karan Bhawsinka (2012)

An extensive look into developing a numerical model for manoeuvring of a planing craft was completed in 2012 by Bhawsinka[8]. In this effort, a Zodiac Hurricane^{TM} Model 733 was modelled, which is 90 centimetres shorter than the vessel tested during this thesis, but with a very similar hull form. The simulation results included a turning circle at 4.5 and 7 knots. The resultant advance (distance travelled parallel to initial track) was 9 and 16 metres and the resultant transfer (distance travelled perpendicular to initial track) was 9 and 15 metres, respectively. Bhawsinksa's results were used as a basis of comparison for the current work, and the results of the simulation compared favourably with the results of the full scale trials presented herein.

2.8 Hui Sun (2011)

In 2011, The Norwegian University of Science and Technology numerically investigated the dynamic response of a planing vessel in head seas [9]. In this effort, "two dimensional plus time" simulations were completed with corrections for three dimensional effects after the fact. These correction appears to work well for Froude numbers above 0.6, which would be the equivalent to 10.4 knots for the subject of this study. The paper showed that the variations in heave and pitch increase as a function of wavelength, as expected, but both reach a maximum around when the wave length is approximately three times the length of the vessels waterline.

2.9 American Bureau of Shipping (2017)

Turning and helm response are of primary interest in this thesis. The American Bureau of Shipping outlines two experiments best suited for this evaluation [10]. The "turning circle" test evaluates the ships' turning ability, independent of helm response. The outputs from this test can be speed-dependent parameters relevant for practicable feedback. Values included are the advance, transfer, and tactical diameter. Two were explained briefly in Section 2.7 and will be fully explored in Section 5.3.1. The tactical diameter is the horizontal distance traveled before the vessels achieves a 180^{o} turn.

Conversely, the zig-zag experiment not only investigates the dynamic response of the vessel with speed, but its immediate reaction to helm input. This experiment involves a number of symetical maneuvers to port and starboard, drawing a zig-zag pattern with the ships track. This will be further explored in Section 5.3.2. Both experiments are conducted as part of this thesis.

2.10 Simon and Litt (2010)

Beyond the experiments, data mining is frequently conducted on the acquired data within this thesis. Simon and Litt at The National Aeronautics and Space Administration investigated methods for steady-state detection of in-flight engine data [12]. While the specific work is somewhat unrelated to the present effort, the algorithm is applicable.

In this method, a state transition logic filter comprised of three stages is used on

incoming real-time data. As data is collected, the mean and standard deviation for a predetermined slice of time is calculated and compared to the running standard deviation. If the standard deviation of the previous time slice is below a certain threshold, the output value for that channel is set to the mean of that time slice. This process continues for the duration of an acquisition. Some additional filters are applied to the data before passing it to the transition logic phase. Low-pass filters, thermal transit filters, and operating regime recognition logic filters were first applied. These attempts to remove slow-transitioning data which would manifest in low standard deiviation but would still yield outliers.

While real-time analysis is not the goal of this project, portions of this filter logic can be implemented when post-processing data that contains considerable scatter.

2.11 Petersen and Winther (2011)

A regressional approach to ship-acquired data was explored in 2011 at the Technical University of Denmark [11] by Petersen and Winther. The investigation argues that the simplicity of the regression method is attractive, but it can be rather laborious to perform. This is true since many factors are inter-related and mutually dependant. These factors may not be immediately obvious to an analyst.

The paper also attempts to create a dynamic model of the ship investigated, using physical data to tune. This allows the model to be extrapolated beyond the measured quantities. While the method works quite well and agrees with the statistical method, the effort involved is beyond the scope of the investigation herein.

2.12 Trodden, Murphy, Pazouki, and Sargeant (2015)

More recently, a harbour tug was instrumented for a month and the data was mined for fuel efficiency purposes [13]. This project, undertaken by Newcastle University in the UK in 2015, is perhaps the most relevant citation to the current effort.

Upon plotting raw fuel and speed data, considerable scatter was observed, demonstrating the need to associate data points with ship activities or other parameters. Various options for analysis were presented by the authors. Smoothing of the data was discarded since the nature of the tug was quite variable and thus short steady state periods with extreme values on either end would be discarded.

Indexing filters were first applied for speed, position, and heading. Only data acquired when the vessel was travelling to and from the dock were considered. Data acquired while the tug was assisting another vessel was discarded due to the dynamics associated with the vessel assisting another.

Applying these filters left steady state values with a relatively small number of transients. The final step was to apply a sorting algorithm which was used to remove the transients. A moving block of constant time width was passed though the speed and fuel consumption data streams, which compared bins of data with its neighbours. Areas of extreme change were thus removed, leaving steady state data. The bin size and tolerance were varied until desirable trends were determined. All plotting, curve fitting, and statical output were then determined from this cleaned data set.

2.13 Summary

From this review of the current literature it is shown that full scale physical data to compliment model experiments is clearly lacking. Sea trial experiments are well defined with sufficient experience and regulations to justify their use as a means for experimentation. Validation and detection of directional stability compared to wave heading is an area to explore to compliment model experiments by Brown and Klosinki (1994) and Hui Sun (2011). The fuel to speed relationship is of much practical use for operators, and its correlation with resistance as explored by Payne (1994) should be of much interest. The methods of data reduction are not trivial. As such, methods to reduce the data to meaningful relationships will be explored in this thesis.

Chapter 3

Vessel and Instrumentation

3.1 Coordinate System Convention

The right hand rule, Z positive down, sign convention is used throughout this report. The datum for vessel locations is the intersection of the transom and keel on centreline.

It is also noteworthy that the rudder angle as prescribed by the sea trials are synonymous to engine angle since this vessel is outfitted with outboard engines which rotate about their mounting structure.

3.2 Vessel

CG 289 is a 8.15 metre rigid inflatable boat, as seen in Figure 3.1, similar to other FRC's used by the Canadian Coast Guard. The hull form is a Zodiac Hurricane^{TM} Model 753. Two Mercury Diesel outboard engines are mounted to the transom for propulsion, as seen in Figure 3.2. All experiments conducted were completed using four blade, 17 inch pitch stock propellers. Both engines were used for all experiments

and thrust was applied equally to both. General particulars of the vessel are described in Table 3.1. Some information is from the vessel's SOLAS stability report [14]. Each test day was started with full fuel tanks to ensure consistent mass properties as far as practically possible.

Figure 3.1: CG 289

Figure 3.2: CG 289 Propulsion Arrangement

Table 3.1: Vessel Particulars

Dimension	**Value**
LOA	8.15 m
B_{max}	2.75 m
$Displacement_{LS}$	2,100 kg
CG_{LS}	(2.118, 0, 0.388) m
$Displacement_{MAX}$	3,823 kg
CG_{MAX}	(2.273, 0, 0.714) m
Fuel Capacity	377 kg

The crew members in a small craft make up a significant contribution to the overall weight and distribution. Table 3.2 shows the weights and centres of gravity of the vessel in the full light ship condition. The general arrangement of the vessel is

shown in Figure 3.3.

Table 3.2: Mass Properties of FRC in Full Load Condition

Property	**Mass (kg)**	**LCG (m)**	**VCG (m)**	**LCG Moment (kgm)**	**VCG Moment (kgm)**
Light Ship	2,100	2.118	0.388	4,447.8	814.8
Pilot	120	2.298	1.342	275.8	161.8
Crew 2	120	1.320	1.342	158.4	161.8
Crew 3	120	1.320	1.342	158.4	161.8
Fuel Tank 1	241	4.675	0.397	1,126.7	95.7
Fuel Tank 2	135	3.043	0.452	413.8	61.5
Total	2,836			6,580.9	
Resultant	2,836	0.513	0.513		1,455.1

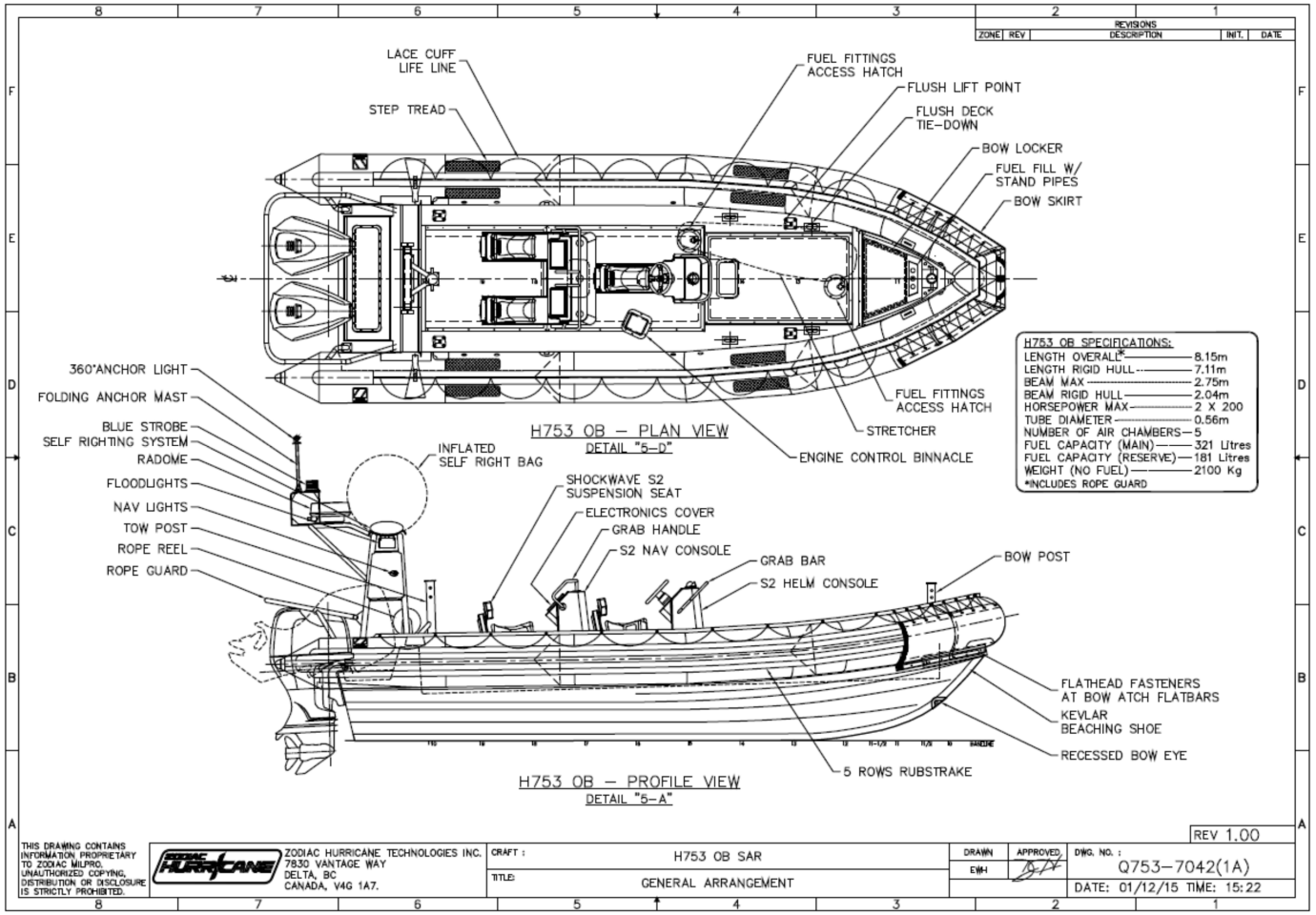

Figure 3.3: General Arrangement

3.3 Instrumentation

Data was acquired from both the vessel and the environment. A data acquisition system (DAS) was installed on board *CG 289* to collect vessel and wind data. Wave buoys were deployed to collect wave data at two test sites, described in Section 3.4. The shipboard system collected from both sensors installed for the trials and pre-existing equipment. Mercury Marine 3.0 L Diesel outboard are provided with the Mercury Smart Craft® system, an engine monitoring system that provides data on engine performance along with GPS position data [15]. A list of all acquired channels considered for analysis is shown in Table 3.3.

3.4 Wave Buoys

The wave buoy deployed at the first test site (Conception Bay South) was moored to the seabed with a soft mooring. This wave buoy was a TRIAXYS™ directional wave buoy, moored at 47.53^0N, 53.08^0W, as can be seen in Figure 3.4. The location was chosen in an area of relatively constant water depth and sufficient distance from the islands in Conception Bay so as to not be influenced by drastic in wave condition and reflections. Due to the age of this buoy, its satellite communication software was obsolete and updating the firmware was a significant investment. A secondary communication protocol was adopted which required a land based acquisition system that communicated with the buoy via VHF radio and limited communication to line of sight. As such, this DAS resided at the author's residence for the duration of the testing since this location was sufficiently close to the testing area.

Table 3.3: Data Acquisition Plan

Channel	**Sample Rate**	**Acquisition System**
SPEED	5 Hz	DGPS
HEADING	5 Hz	DGPS
ROLL	160 Hz	DMU Inertial Sensor
PITCH	1605 Hz	DMU Inertial Sensor
STEERING ANGLE	5 Hz	Independent DAS
TEMPERATURE	0.5 Hz	NMEA
LONGITUDE and LATITUDE	10 Hz	DGPS
WIND DIRECTION	4 Hz	Doppler Anemometer
WIND SPEED	4 Hz	Doppler Anemometer
ROLL RATE	160 Hz	DMU Inertial Sensor
PITCH RATE	160 Hz	DMU Inertial Sensor
YAW RATE	160 Hz	DMU Inertial Sensor
X, Y, and Z ACCELERATION	160 Hz	DMU Inertial Sensor
COURSE	10 Hz	NMEA
SPEED N2K	10 Hz	NMEA
LONGITUDE and LATITUDE	10 Hz	NMEA
BATTERY VOLTAGE	0.5 Hz	NMEA
PORT and STBD ENGINE RPM	10 Hz	NMEA
PORT and STBD ENGINE TILT	10 Hz	NMEA
ALTERNATOR VOLTS	10 Hz	NMEA
PORT and STBD FUEL COMP	10 Hz	NMEA

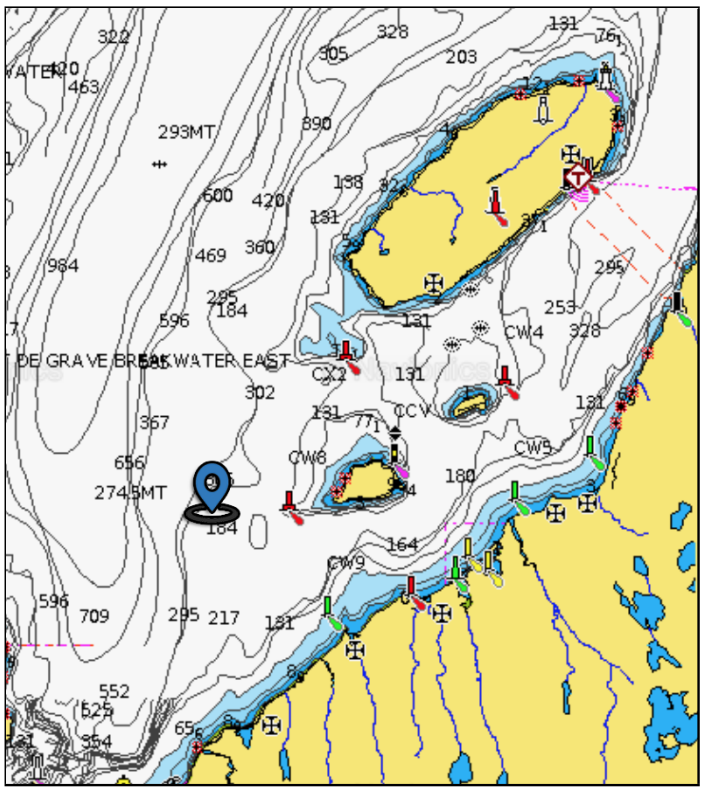

Figure 3.4: Wave Buoy Location

The second test site, just outside St. John's harbour, was only used for a single day. In this case, a smaller version of the TRIAXYS^{TM} wave buoy was deployed upwind of the test site, allowing it to drift through the test area, and was retrieved after testing was completed. The specifications for the wave buoys are included in Appendix A.

Chapter 4

Test Plan

4.1 Introduction

The tests completed are grouped into four categories: manoeuvring, acceleration, towing, and seakeeping. Different types of test were used to evaluate the areas which are outlined in the following sections. The full DAS recorded all channels for every test, adding to the cloud of data explored in detail in Chapters 5 and 6.

4.2 Manoeuvring Tests

To assess manoeuvring, two types of tests were employed: turning circles and zig-zags. The guidelines for these tests were taken from the American Bureau of Shipping [10]. Since these guidelines are designed for a much larger ship, slight modifications were required to better serve this type of vessel. These modifications, where they arise, are described throughout this report.

4.2.1 Turning Circles

This test is used to measure the time and distance it takes for a vessel to complete a turn. During this manoeuvre, the vessel should be travelling at a constant desired speed. The rudder is then positioned hard over until the original heading is achieved, completing a full circle. This is completed for both port and starboard directions. The outboard engines on this vessel are capable of large angles, and at high speeds, capsizing is a possibility. As such, the helm angle was thus defined as the tightest turn possible at which the desired speed could be maintained safely based on the helmsman's experience. From the GPS data, the indicative parameters obtained from this manoeuvre are the tactical diameter, advance, and transfer as described in Figure 4.1.

The turning circle test was completed for 5 speeds in total: 4, 8, 20, 30, and 38 knots. Full throttle dictated the final speed of this set. For the two lowest speeds, the helmsman was able to achieve hard over on the wheel, which equates to 24^{o} steering input. For 20 and 30 knots, 10^{o} of rudder was achieved, and for full throttle, 7.5^{o}.

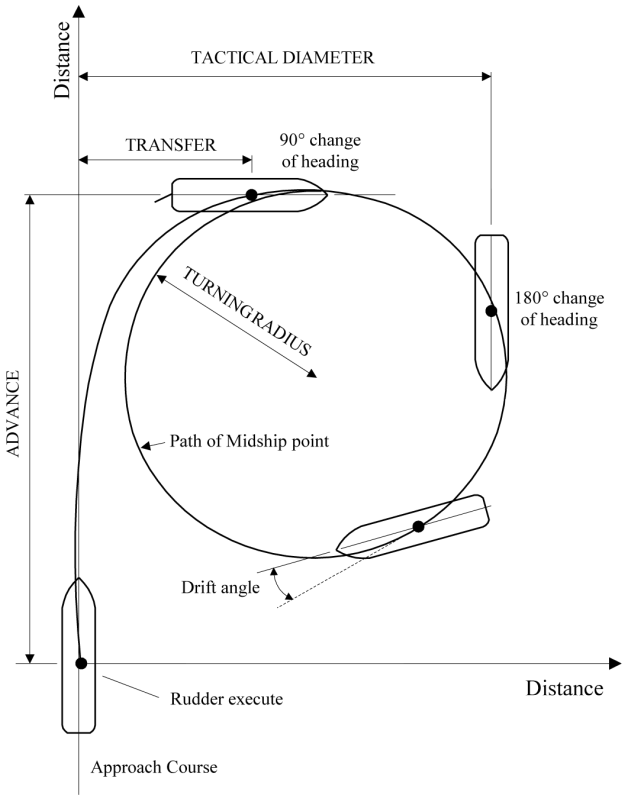

Figure 4.1: Turning Circle Test Parameters

4.2.2 Zig-zags

Zig-zag tests are a more dynamic method of testing a ship's reaction to helm input. In this test, yaw rates are included as part of the test and the ship's reaction to them is assessed. At the beginning of the test, the vessel is brought up to the desired speed. Next, the engines are set to a certain angle and the vessel reacts. When the vessel's heading reaches that of the engine angle, the engine angle is changed to steer to the opposite side. For example, consider a 10° zig-zag. The vessel is first brought up to

speed and the helm is set to 10° to starboard. The vessel thus starts to turn. When the vessel's heading reaches 10°, the helm is set to 10° to port. When the vessel's heading reaches -10°, the helm is set to 10° to starboard, and so on.

Two angles were chosen to be assessed, 10° and 20°. The 10° case was tested at 4, 8, 20, 30, and 38 knots. The 20° case was only tested at 4 and 8 knots for safety reasons. The indicative parameters obtained from the zig-zags are described in Figure 4.2.

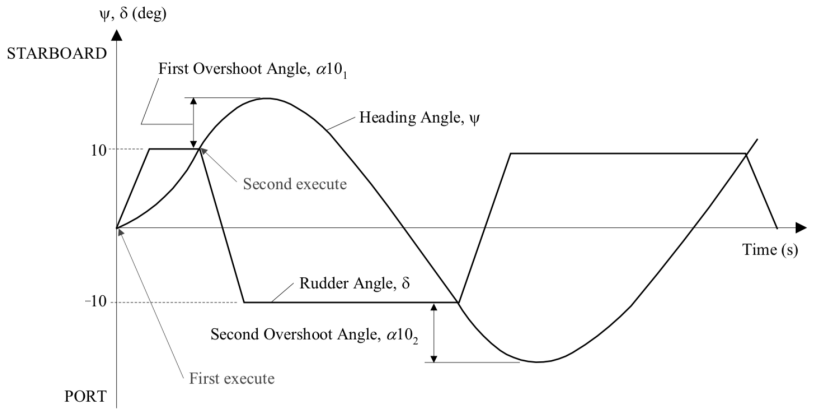

Figure 4.2: Zig-zag Test Parameters

4.3 Acceleration

Propulsion power was assessed to determine this vessels ability to achieve maximum speed with respect to time and distance. Natural deceleration (no throttle input) was also assessed.

4.3.1 Standing and Rolling Starts

Acceleration tests were conducted to assess the vessel's ability to reach maximum speed from standing (standing start) and acceleration from speed (rolling start). The speeds chosen for the rolling starts were 4.0, 8.0, and 20.0 knots. These tests were performed in calm water and repeated for both upwind and downwind conditions, even though wind conditions were very light (less than 5 knots) during these tests.

4.3.2 Deceleration

At the end of the standing start, once full speed was achieved, the throttles were pulled back to neutral and the vessel decelerated naturally. The distance and time to reach zero speed were recorded.

4.4 Towing

To assess the towing capacity of the vessel, two tests were performed: a bollard pull test, which measures the thrust developed when the vessel is tied to a bollard on a dock and a tow experiment, where the tension in a tow line was measured while towing another vessel..

4.4.1 Bollard Pull

A bollard pull is a zero speed test to determine the thrust developed by the main engines at various engine speeds. In this test, a load cell is fitted between a static structure and the vessel. The engines are then throttled through their operating range

in steps of 500 rpm. To detect hysteresis in the setup, the engines were slowed down to idle in steps of 1000 rpm.

CG 289's tow line was used for this pull. The static structure was a piling on a wharf, and was approximately 50 metres from the vessel during the test. Figures 4.3 and 4.4 below detail the bollard test setup.

Figure 4.3: Bollard Pull Setup (1 of 2)

Figure 4.4: Bollard Pull Setup (2 of 2)

4.4.2 Towing

To better quantify the towing capacity of *GC 289*, a tow of a vessel that is representative of a typical tow during rescue operations was undertaken. The *F/V Roberts Sisters II* was towed for approximately 1 nautical mile. The *Roberts Sisters II* is a 19.7 meter fishing vessel with beam of 7.01 meters a gross registered tonnage of 127 tonnes [16].

The tow was completed in St. John's harbour with minimal wave action. The wind varied from 15 to 20 knots from the SW for the duration of the experiment. Similar to the bollard pull, the throttle was varied throughout the experiment. While this experiment was completed both upwind and downwind, only the upwind portion was analysed due to segments of missing data (or dropouts) in the downwind data. These dropouts are discussed in Chapter 8.

4.5 Seakeeping

The last category of tests completed was to assess the seakeeping characteristics of the vessel. A star pattern manoeuvre was chosen to best capture the vessel's motions in various headings relative to the direction of wave propagation. In this manoeuvre, the vessel is driven in a series of constant speed legs and headings in sequence, effectively "drawing" a star pattern, as illustrated in Figure 4.5. This is completed by turning both to port and starboard leading to a total of ten target angles relative to the wind, listed in Table 4.1.

These patterns were performed in three wave conditions and at various speeds, summarized in Table 4.2. Note that the term wave condition refers to distinct differences in wave statistics for various phases of testing and is not in reference to the Beaufort scale.

For many reasons, not all tests were completed. At 20 knots in wave condition 1, there were concerns about excessive propeller ventilation due to the vessel skipping over the short steep waves and thus the two higher speeds were not attempted. In wave condition 3, the uncompleted tests were a result of the day being cut short due to worsening weather conditions and concerns for crew safety.

The intention was to have all legs occur for the same duration, but the larger speeds were cut short due to restrictions in the operational area. Additionally, there was some difficulty in maintaining the desired headings due to delays in feedback response of the GPS system. The data was analysed and the actual achieved heading was determined for use in subsequent analysis.

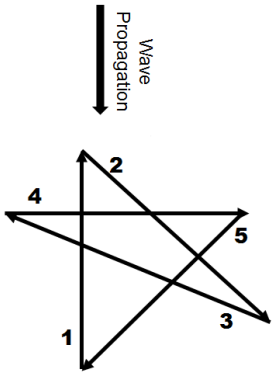

Figure 4.5: 5-Leg Star Pattern

Table 4.1: Star Angles

Leg	**Angle**
1	0º
2	150º
3	300º
4	90º
5	225º
6	180º
7	45º
8	270º
9	120º
10	330º

Table 4.2: Star Pattern Test Matrix

Speeds (knots)	**Wave Condition 1** Hs 0.52m, Tp 2.71s	**Wave Condition 2** Hs 0.4m, Tp 6.51s	**Wave Condition 3** Hs 3.6m, Tp 11.9s
4	✓	✓	✓
8	✓	✓	
20	✓	✓	✓
30		✓	
38		✓	

Chapter 5

Analysis

5.1 Introduction

The bulk data analysis for the test data was completed using an object oriented analysis code developed by the author within the Maltab© software environment. The analysis can be grouped in two categories: pre and post processing. The following sections outline all analysis procedures within these two categories.

5.2 Pre-Processing

The pre-processing routines were run on all data sets. These routines include translations and various cleaning, as required, for all data and they are described below in the order they occur during the actual analysis.

5.2.1 Data

For every acquisition, the DAS outputs a series of files according to each channel as previously outlined in Table 3.3. Each file contains the data for the associated channel and time of acquisition. Acquisitions start and stop with the vessel's engines.

Every set of files was loaded in the Matlab environment whether or not a test as described in Chapter 4 was performed during that acquisition period. All data contributes to the total data set comparisons further explored in Chapter 6. Since the data formats for different channels are very different and sometimes time consuming to load, the data was immediately saved to a harmonized file. Subsequent loading of this data was from harmonized file rather than performing the time intensive task of loading and combining individual files. A directory was created with the date and time of the acquisition and was used for storing data throughout this analysis procedure.

5.2.2 Despike

The engine temperature, latitude, and longitude data from the NMEA system have sporadic spikes in the data. To address this, the time-derivative of these channels was computed. Any value exceeding twice the standard deviation of this derivative was removed. These gaps were then filled using a Piecewise Cubic Hermite interpolation. This method lends itself well to ship type motions while preserving the monotonicity of the data streams [17]. It is also noteworthy that these spikes are very short in duration, on the order of 0.1 seconds, and thus the interpolation is considered non-intrusive.

5.2.3 Course Corrections

Next, the course measured by the NMEA system was corrected to account for discrepancies in the sensor. This sensor outputs data from -180° to +180°, where 0° indicates north. As such, if the vessel was travelling on a southern heading, the value would change +/- 180° relatively quickly. The sample rate of the system is faster than the time it takes for the analog signal to switch from positive to negative, as such, erroneous data during the switch was recorded. Consider the plot in Figure 5.1, a graph of the course as the vessel turns through a southern heading. At the point where it is nearly due south, combined with variations in the course due to wave action, there exists data between +/- 180° which do not represent the vessel's actual course.

To accomplish this correction, the data was first split into individual cartesian components by a typical sine and cosine calculation. Next, these components were split into equally-spaced intervals, each being nine datapoints long. The median of these intervals along with its associated time value (the centre of each interval) was calculated. The original signal was then calculated using Maltab©'s inverse tangent function, "atan2". This differs slightly from a typical inverse tangent in that the results are placed in the appropriate quadrant [18]. The resultant correction of the previous example can be seen in Figure 5.2.

After completion of this process, to better align with standards of naval navigation, all values between -180° and 0° are converted to compass headings from 180° to 360°.

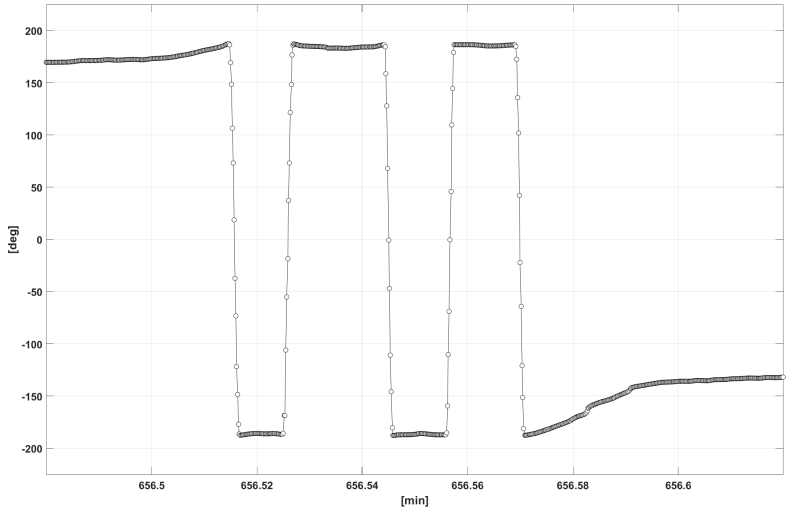

Figure 5.1: Example Course, Before Correction

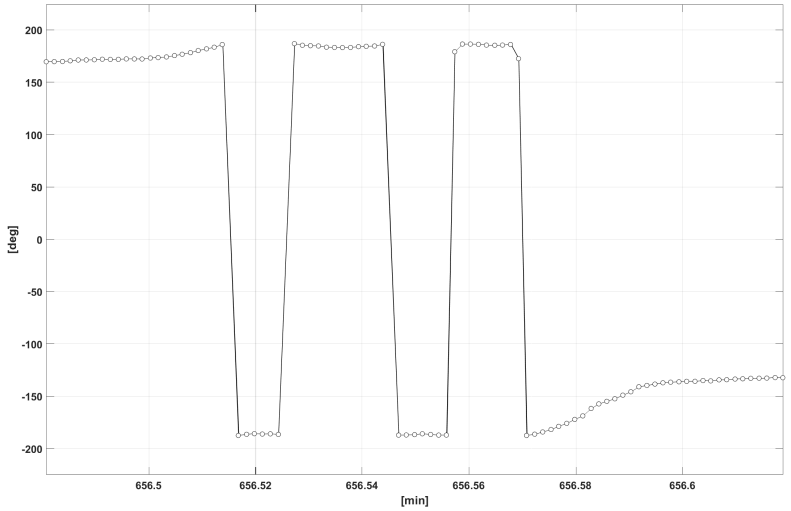

Figure 5.2: Example Course, After Correction

5.2.4 Time Series Plotting

Next, time domain plots of all channels (five channels at a time) were plotted such that any quality issues with the data could be discerned. Any drift or erroneous values were addressed and added to the analysis procedure. In fact, the routines described in the preceeding sections are a result of these inspections. As new analysis procedures were developed the all data was reanalyzed to include all additions. The resultant plots were saved in the appropriate directory.

5.2.5 Fuel Consumption

The fuel consumption data for each main engine was acquired. A new time series data stream was calculated by a simple addition of these two parameters to compute total fuel consumption.

5.2.6 Location Plot

An animation and plot of the vessel's location was the next stage in analysis. The location of the vessel was indicated as a dot upon a bathymetric marine chart for every 5 second interval. This serves to verify the latitude and longitude positional readings as the time series of this type of data is not easily discernible. Additionally, one can calculate the approximate speed of the vessel based on the spacing of the dots.

5.2.7 Data Segmentation

The data was split into relevant segments required for further analysis. Since all channels of data were recorded from the point of engine start to the point of engine shut down, not all collected data is relevant for each type of test. For example, consider the towing pull as described in Section 4.4.2; for this test type, statistics of each constant speed section of the test are of interest since the relationship between fuel, engine speed, and vessel speeds can be inferred solely by means of the segments.

To accomplish this, the latitude and longitude data was presented to the user on a similar plot as in Section 5.2.6 with some additional user interfaces. The user was presented with a slider bar, starting at time 0 and ending at the time at which the acquisition ended. As the bar is moved, the associated position of the vessel is portrayed on the plot. Combined with a start/stop toggle, the user can selected portions of the vessel's track to isolate for analysis. Figure 5.3 shows an example of such a screen with 3 segments selected. Once completed, the data was split into the number of segments selected based on the start and stop time indices.

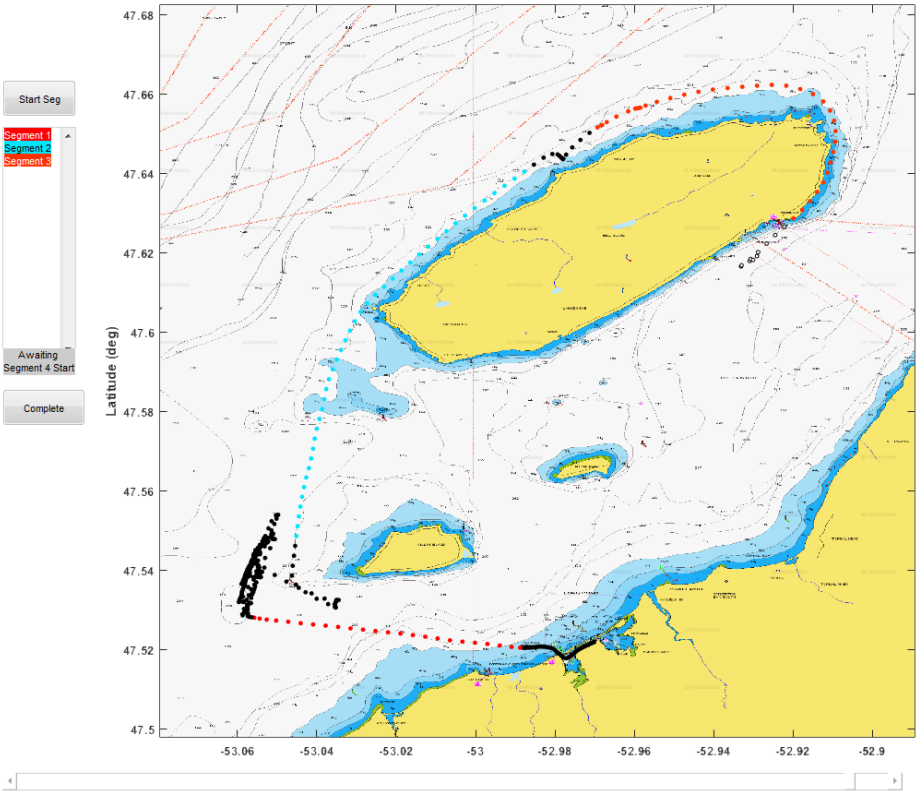

Figure 5.3: Example of Interactive Segment Selection

5.2.8 Statistics

The mean, maximum, minimum, range, and standard deviation for all channels and data that lie within each respective time segment were calculated and added to the database.

5.2.9 Data Export

All data was saved in a variety of formats. First, the data was saved as a Matlab© MAT file, to be used for future post-analysis and loading of historical data. Additionally, statistics calculated during the analysis were saved to a comma-separated variable (CSV) file.

5.3 Post-Processing

Once all pre-processing was completed, the post-processing commenced. These routines are test type dependant. However, not all types of tests were sufficiently complex to warrant an independent post-processing routine. For example, in the cases of the towing and bollard pull experiments, segmentation and statistics as described in Sections 5.2.7 and 5.2.8 were sufficient to produce the required results. Each post-processing routine developed and used for analysis is described in the following sections.

5.3.1 Turning Circles

Once the associated segments was selected, they were processed using the turning circle analysis routine. From the output from that routine, the parameters as defined in Section 4.2.1 and Figure 4.1 were determined, as described by the following sections.

5.3.1.1 Advance and Transfer

The vessel's initial course must first be tared out, that is, subtracted from the entire course signal such that the vessel's track appears northward immediately before the

turning circle. This greatly simplifies the analysis routine as the circles are oriented the same way for each analysis. Once the engine angle has changed by 1°, the turn was deemed to be started. When the course has reached +/- 90°, the time stamp was recorded. The *advance* and *transfer* was then calculated.

The *advance* is the distance travelled from the first indication of engine angle change to the time at which the vessel reached 90°. The *transfer* is similar, but it is the distance travelled perpendicular to the vessel's initial track. From the known GPS data, the Matlab© distance function was used to calculate the arc length over the surface [19].

5.3.1.2 Tactical Diameter

As the vessel continues to turn, the time corresponding to a 180° heading was recorded. The perpendicular distance between this point and the first indication of engine angle change was recorded as the *tactical diameter*.

5.3.1.3 Turning Radius

Finally, the *turning radius* was calculated by recording the time at which the vessel's heading matches that of its initial heading. The distance from this point to the 180° point was calculated and recorded as the *turning radius*.

5.3.1.4 Export

The compiled results were recorded in a MAT file, along with the other turning circles. This data was saved to a CSV file similar to that described in Section 5.2.9. Also, the excerpt time series data for all channels during the turn was exported and saved

similar to the manner described in Section 5.2.9. Finally a diagram of the vessel's position was recorded, as seen in the example in Figure 5.4. Note the data shown in Figure 5.4 shows the true, not tared, course.

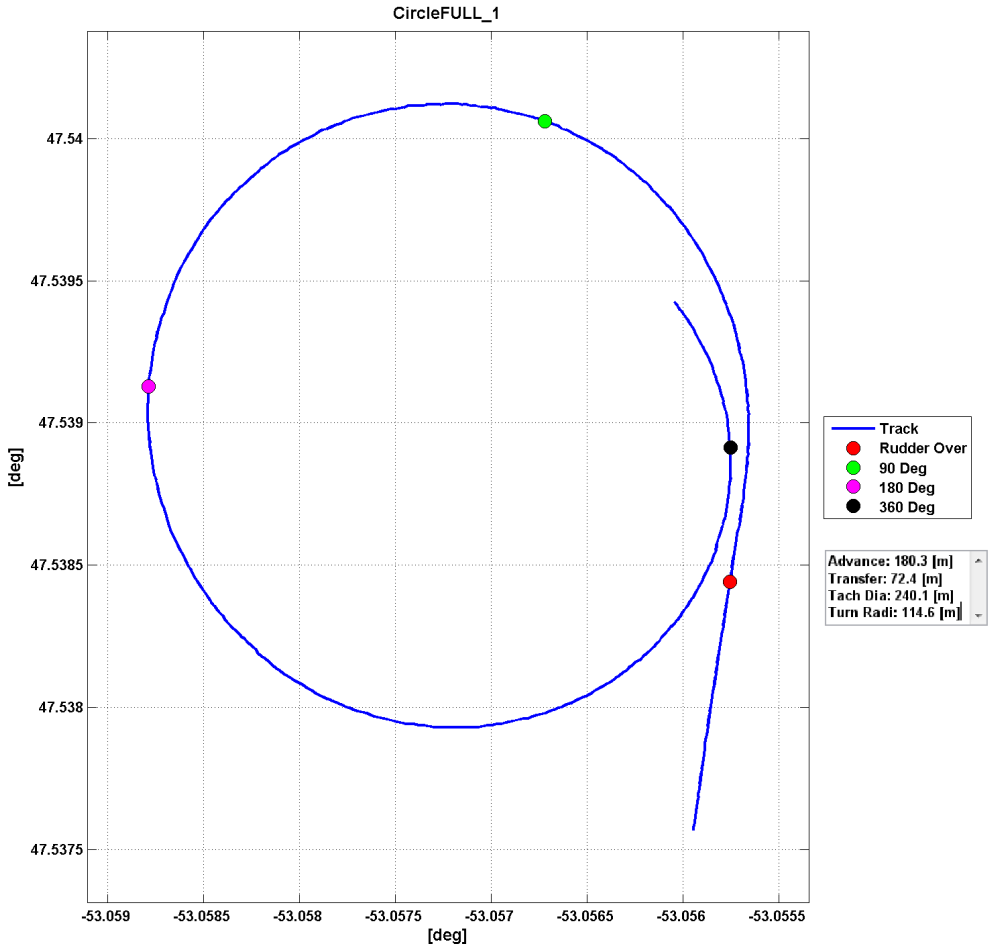

Figure 5.4: Example of Vessel Position Plot for Full Speed Turning Circle (True Course)

5.3.2 Zig-zags

Similar to the turning circles, the zig-zag tests were analyzed using case specific routines. The relevant sets of data were passed to it and the parameters were determined as defined in Section 4.2.2 and Figure 4.2, as described below.

5.3.2.1 Overshoot

The first value calculated is the maximum heading that was achieved after the second execution of the engine angle. In other words, when the zig-zag pattern was initialized, the engine angle was set to a value, 10° for example. When the heading read 10°, the engines were turned to to -10°. The rotational and linear momentum of the vessel means that there was a delay between rudder execution and heading response. This delay manifests itself as an *overshoot*. To calculate this, a zero-crossing analysis routine was performed on the heading channel recording crossover indices and maxima of the signal. The *overshoot* is simply the value of the first maxima.

5.3.2.2 Reverse Rudder Heading Angle

Since it takes time to switch the engines to the other side by physical rotation of the helm, there is a discernible heading change between initiating the turn and arriving at the target helm angle. The time at which the engine angle reached its setpoint was determined and the associated heading angle and its time recorded as the *reverse rudder heading angle*.

5.3.2.3 Reach and Cycle

The *reach* and *cycle* were calculated next based upon the zero crossing analysis completed in Section 5.3.2.1. These values are the time and distance from start to complete a half cycle and full cycle, respectively.

5.3.2.4 Export

Similar to Section 5.3.1.3, the data was saved to a MAT file and exported to a CSV file. A GPS plot and animation was also completed, as seen by the example in Figure 5.5.

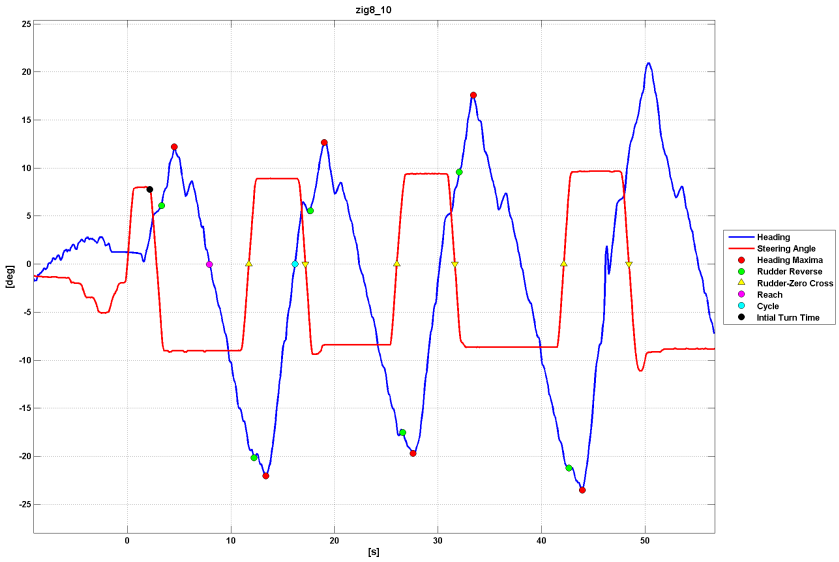

Figure 5.5: Example of Vessel Position Plot for a Zig-zag Test

5.3.3 Star Patterns

The final post-processing routine that is sufficiently complex to require its own case specific routine is the star patterns. In this routine, data for an entire star was passed to the script. The port and starboard turns were treated as a single maneuver for this analysis. Section 4.5 and Figure 4.5 outline the test plan for star patterns.

5.3.3.1 Relative Course

Since one of the primary purposes of the star pattern is to determine the vessel's performance at various angles relative to wave propagation, a new course channel was calculated. The course data received from the GPS was relative to true north. This was corrected by simply subtracting this course from the wave propagation direction (determined by observation) to calculate a relative-to-wave course.

5.3.3.2 Segmentation and Statistics

Similar to section 5.2.7, the star patterns were displayed to the user by the software's graphical user interface and the appropriate legs are selected and segmented. The mean, max, min, and standard deviation were then calculated for each leg.

5.3.3.3 Polar Plots

Since the data from the star patterns were completed on a variety of headings, polar plots were generated to better assess the nature of the statistics. These plots were generated after all series of star patterns were analysed such that all statistics for a single channel could be portrayed on a single plot. Consider the example in Figure 5.6; this polar plot shows the standard deviation of the roll channel on the radial

axis and the achieved heading relative to wave on the tangential axis. It can be seen from the plot that, as expected, the standard deviation of roll increases as the relative heading approaches more abeam. These results are further explored in Section 6.6.

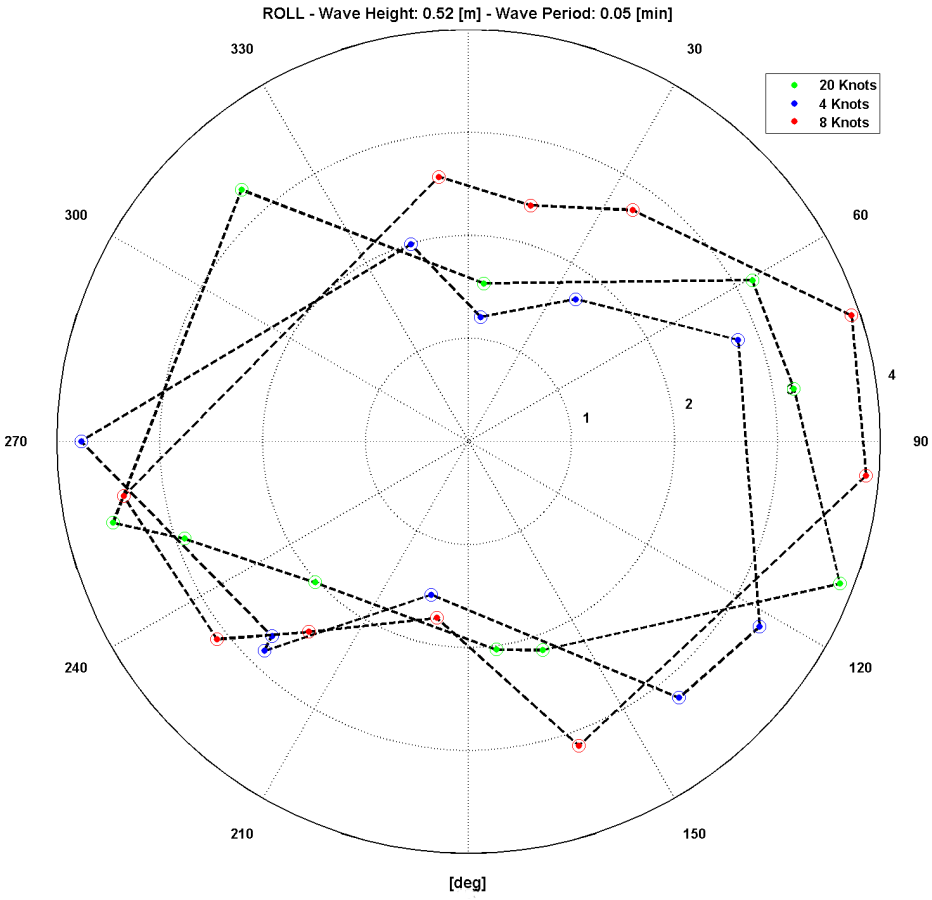

Figure 5.6: Example Polar Plot of Standard Deviation of Roll

5.3.4 Performance Curves

As discussed in Section 4.1, the acquisition system installed on the vessel was active and recording whenever the vessel was operational. As a result, much data was captured for a variety of scenarios. The following sections describe the data filtering that was performed to produce the best confidence in the extracted performance curves.

5.3.4.1 Initial Review

Initial attempts were made to determine trends in parameters which were expected to be correlated. For example, speed vs. fuel consumption should yield a reasonable correlation. Plotting all the data points, however, shows considerable noise in the data as is obvious in Figure 5.7.

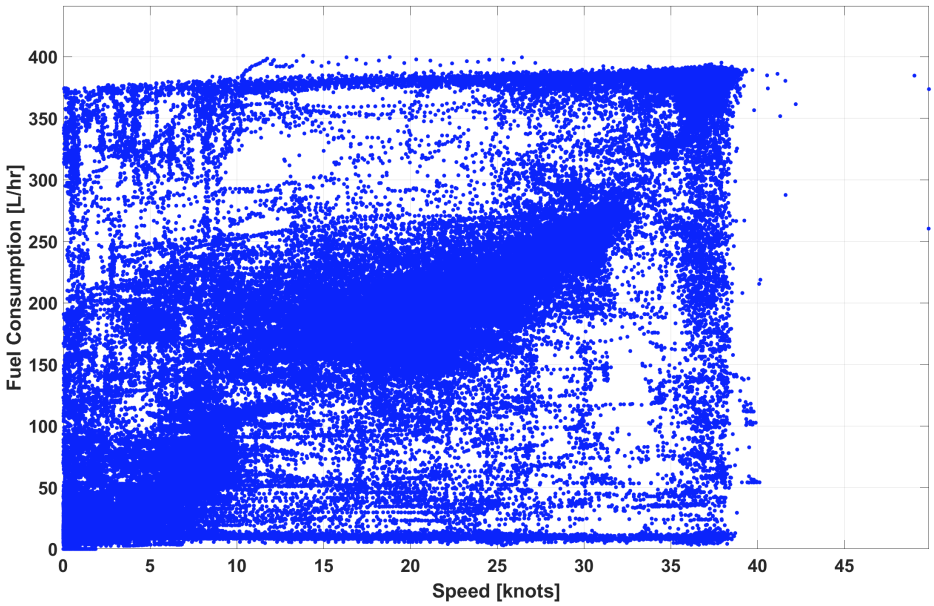

Figure 5.7: Fuel Consumption vs. Speed

Plotting the fuel consumption against the engine rpm shows a more reasonable correlation, but still higher than desirable noise as can be seen in Figure 5.8. It was evident that further filtering was required. This was not completely unexpected, as presented by the data presented in by Newcastle University [13] However, the scatter is much higher than was observed during that investigation. This is likely due to the much higher sample rates used in the current research ranging from one data point for every two seconds to 160 data points per second versus the one data point every 60 seconds in the Newcastle effort.

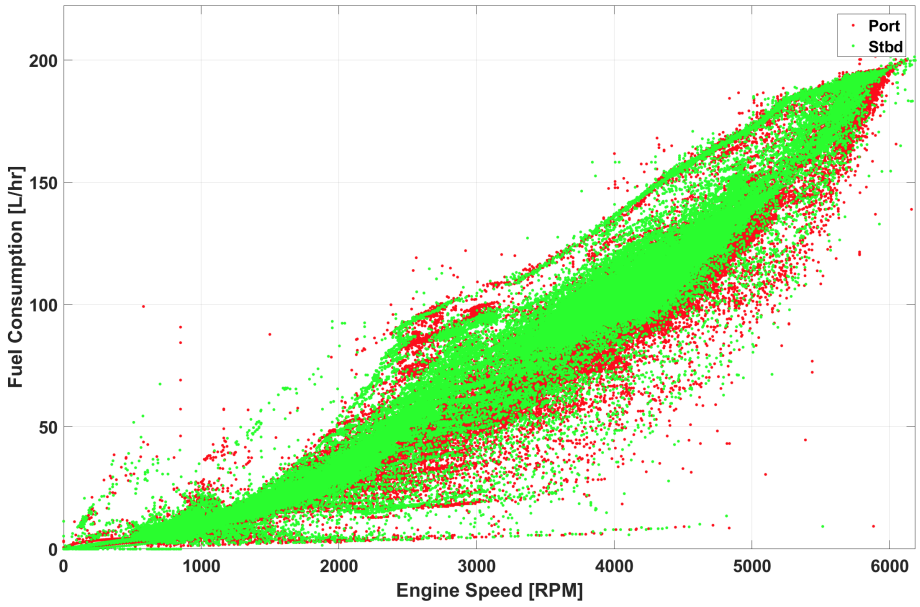

Figure 5.8: Fuel Consumption vs. Engine Speed

In an attempt to discern the source of the noise, Figure 5.7 was re-plotted with a color specification for forward motion acceleration. This acceleration was calculated by a point-by-point differentiation of the speed data. The result is seen in Figure 5.9.

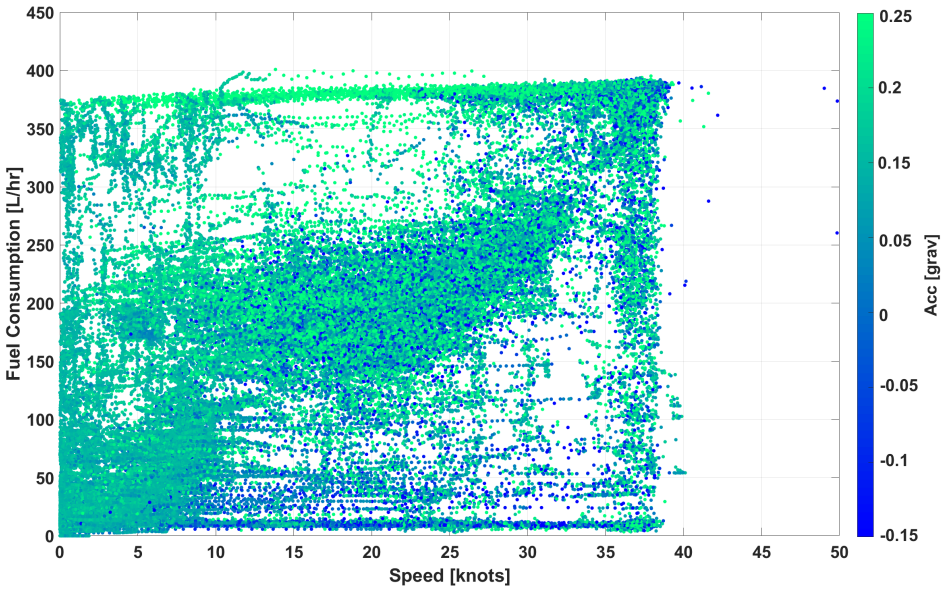

Figure 5.9: Fuel Consumption vs. Speed vs. Acceleration

By inspection of this plot, one can see the extreme high values (high fuel consumption, low speed) occur during forward acceleration, and the extreme low values (low fuel consumption, low speed) occur during deceleration (coasting).

Similarly, Figure 5.8 was re-plotted with vessel speed as the color specification as seen in Figure 5.10.

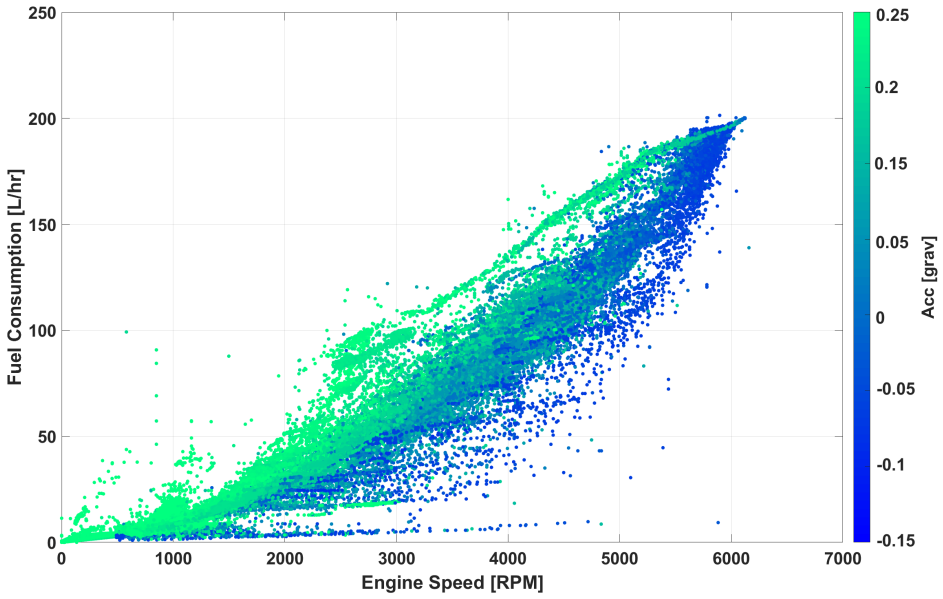

Figure 5.10: Fuel Consumption vs. rpm vs. Acceleration

It is clear from this plot that higher and lower fuel consumptions for a given speed are dependent on acceleration. As such, a technique must be employed which filters out transient effects on the data before global performance curves can be deduced.

This technique must not only remove transient effects of speed but any other parasitic influence on the system. For example, if the vessel was travelling at a constant speed but there was significant engine angle input, then the fuel consumed during this duration of time would not be representative of a steady state value. Likewise, during acceleration, the engine speed and fuel consumed may be constant but the varying speed would yield unrealistically high engine consumption not indicative to any particular speed, as has been demonstrated above.

Note that this filtering fundamentally differs from any analysis completed during

pre-processing in that the data was not being modified, but rather a subset of the data was being selected. This data reduction technique is discussed below.

5.3.4.2 Sub Segmentation

A statistical method, dubbed sub segmentation, was developed by the author to filter out transient effects. This method combines various aspects of those employed by NASA and Newcastle University explored in Sections 2.10 and 2.12.

Variations of the parameters in this method were undertaken until the data was qualitatively clean. The purpose was to reduce the data to only contain steady-state signals; not only steady-state with respect to its own value, but steady-state throughout the entire set of channels.

The first step in this method was to split the data for each channel in equal time lengths. This time length was iterated until a value of 5 seconds was determined to be most reasonable. These bins of data may be different sizes depending on the sample rate, but the start and end time index for each was the be the same.

Next, the mean, standard deviation, and time centroid for each bin was calculated. The purpose of calculating the standard deviation was to assess the variability of the signal within that bin. The standard deviation for each signal was then sorted from smallest to largest and the index of the top 30% for each signal was recorded. Consider Figure 5.11 where the green areas show the segments of low standard deviation. Note that this graph shows about 3,120 sub segments.

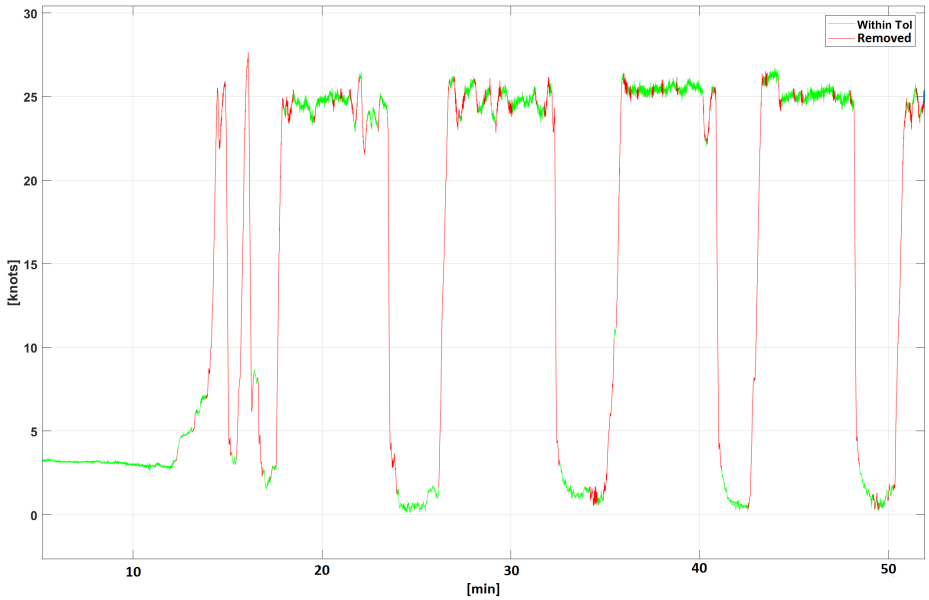

Figure 5.11: Speed Sub Seg Excerpt

After the low standard deviation segments had been determined, each sub segment was compared for each channel and those sub segments which showed a low standard deviation across each channel were retained. In other words, for each five second interval, only those intervals that showed low variation for each and every channel were retained, and the remaining were discarded. Figure 5.12 uses the same data set as 5.11 but only illustrates the sub segments which were steady state for all channels.

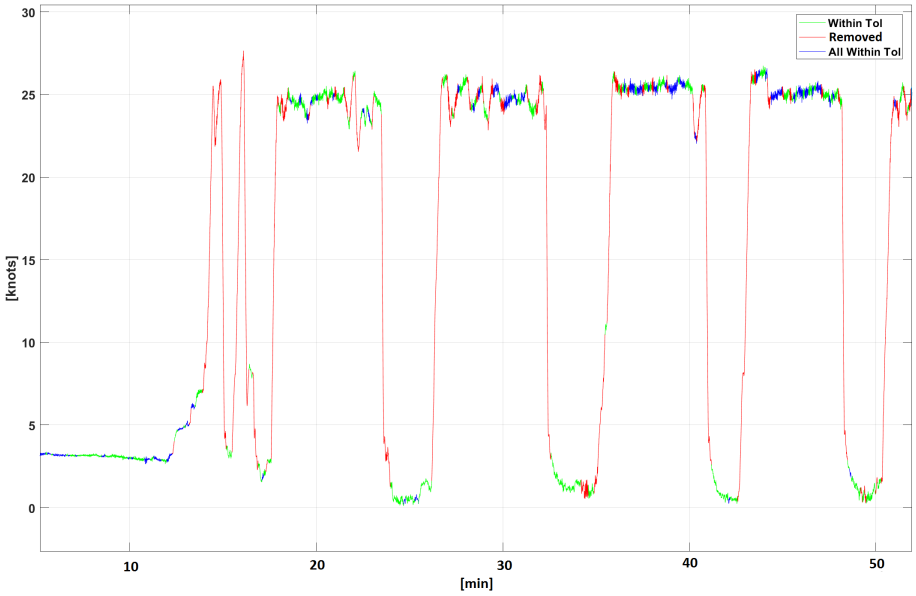

Figure 5.12: Speed Sub Seg Excerpt, Low Standard Deviations

Note that the mean value for each sub segment was retained rather than the individual datapoints within the sub segment. Through this process, 5% of the entire data sampled remain, but it is within this 5% that reliable curves and correlations can be obtained.

The performance curve results are presented in Section 6.7, but as a point of validation of this method, re-consider the initial graph in Figure 5.7. This graph is plotted below in Figure 5.13 using the data after the sub segment filter has been applied. This plot now represents a speed vs. fuel consumption (analogous to resistance) plot relationship that one might expect from a planing craft, with its distinct displacement resistance below 10 knots, a transition area between 10 and 15 knots,

and a planing curve from 15 knots onward.

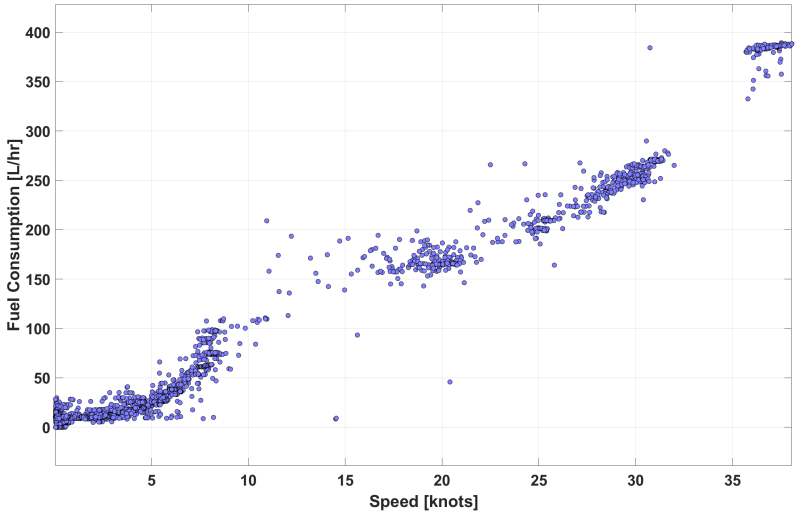

Figure 5.13: Fuel Consumption vs. Speed

Chapter 6

Results and Discussion

6.1 Introduction

The post-processing results as obtained using the methods described in Section 5.3 are outlined and discussed in the following sections; results are presented in the same order as the analysis methods described in Chapter 5.

6.2 Turning Circles

As a reminder, the turning circle diagram is replicated in Figure 6.1. The experimental results are detailed in Table 6.1

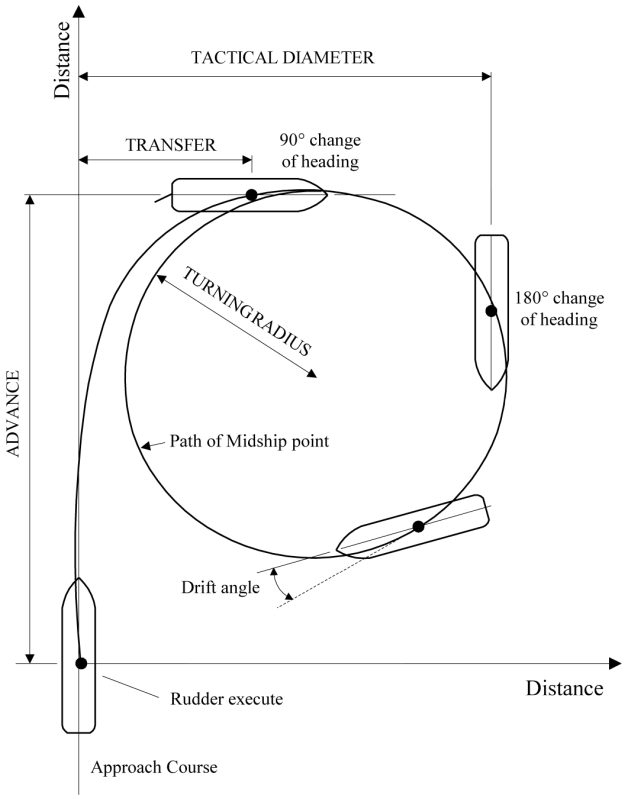

Figure 6.1: Turning Circle Parameters

The trends follow as expected when compared to speed. Each trend is plotted below in Figures 6.2 to 6.5. In general, the vessel can execute a full about face turn in just over 200 metres at full speed (38 knots) and just under 20 metres at a manoeuvring speed. The vessel also travels about 75% of this distance in the direction it was initially travelling from the point of first rudder execution.

Table 6.1: Turning Circle Results

Speed	**Advance**	**Transfer**	**Tactical Diameter**	**Turning Raidus**
knots	metres	metres	metres	metres
4	17.2	4.45	17.85	7.15
8	19.5	1.4	23.1	7.9
20	57.9	34.35	93.8	50.6
30	86.95	51.25	136.75	72.35
38	146.35	90.6	208.7	108.75

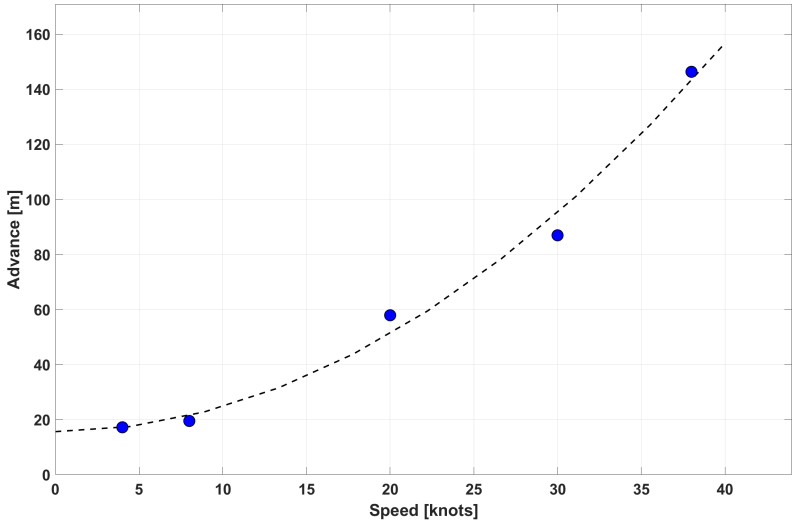

Figure 6.2: Advance vs. Speed

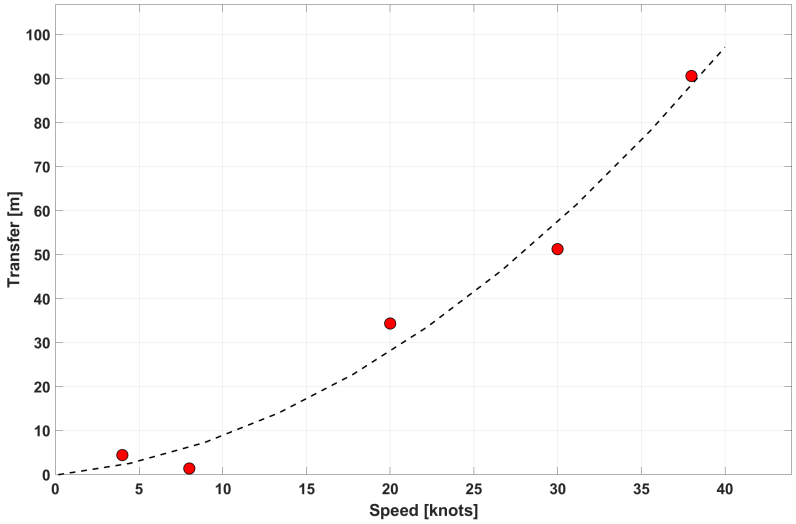

Figure 6.3: Transfer vs. Speed

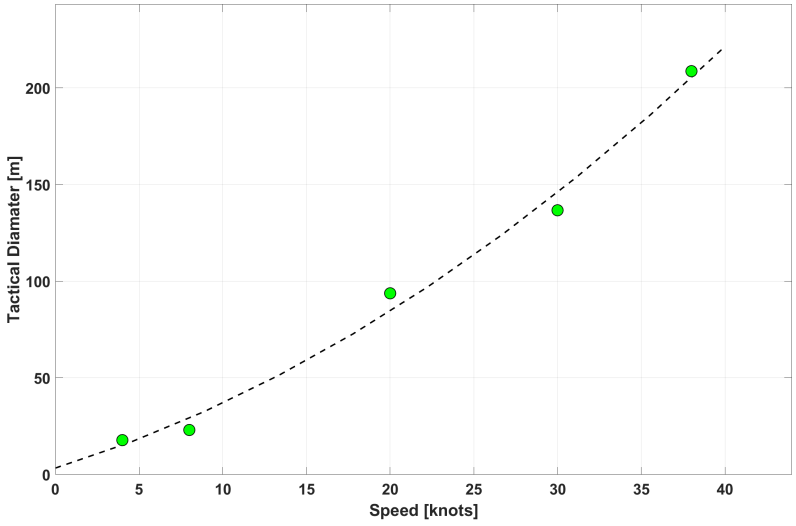

Figure 6.4: Diameter vs. Speed

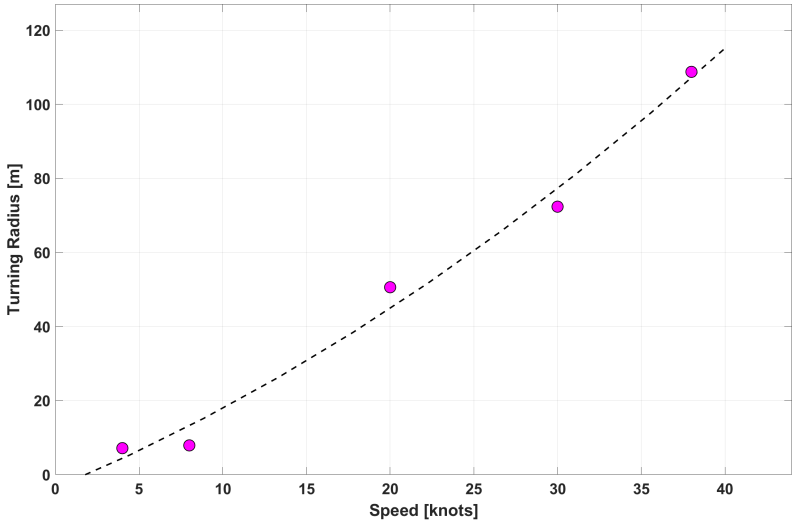

Figure 6.5: Turning Radius vs. Speed

It is noteworthy that some turning circles exhibit an elliptical shape. This variance was compared as a percentage difference between the major and minor axes of the ellipse, as seen in Table 6.2. At most, the variation was 6.2%. The wind during these turning circles was 7 knots, and thus not likely the source of the discrepancy. Other contributing factors could be the vessel skidding, or it may also be operator induced. GPS track plots of the turning circles can be found in Appendix B.

Table 6.2: Turning Circle Ellipsoid

Speed	**Ellipsoid percentage**
knots	%
4	4.8
8	4.3
20	7.0
30	6.2
38	3.7

6.3 Zig-zags

The Zig-zag tests were arguably the most difficult to execute according to plan due to the quick response of the vessel. The magnetic compass used on this vessel caused a feedback lag to the pilot. Slower moving ships make instrumentation lag negligible and also allow for precise rudder action. As a result, the pilot used distant landmarks predetermined to be at the appropriate heading for each test.

The parameters as described in the Zig-zag diagram are presented in Figure 6.6. Again, as a reminder, the figure is replicated in Figure 6.6. The experimental results are detailed in Tables 6.3 and 6.4.

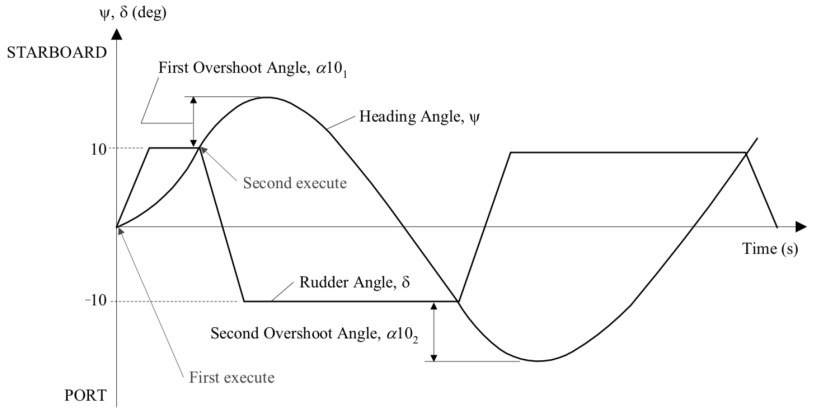

Figure 6.6: Zig-zag Parameters

Table 6.3: Zig-zag Results - 10 degree

Speed	**4 knots - 10°**	**8 knots - 10°**	**20 knots - 10°**	**30 knots - 10°**	**38 knots - 10°**
Initial Turn Time [s]	2.22	2.17	2.20	1.42	2.07
Rudder Reverse [deg]	2.54	6.10	8.87	11.6	12.6
1st Overshoot [deg]	-5.94	2.21	-0.838	3.52	6.89
2nd Overshoot [deg]	-1.01	12.1	0.845	-0.894	-5.41
Yaw Check [s]	2.00	2.36	1.18	0.910	0.620
Reach [s]	5.54	7.93	4.79	4.05	5.12
Cycle Time [s]	10.8	16.2	8.21	7.05	7.01

Table 6.4: Zig-zag Results - 20 degree

Speed	**4 Knots - 20°**	**8 Knots - 20°**
Initial Turn Time [s]	5.42	3.09
Rudder Reverse [deg]	31.5	42.3
1st Overshoot [deg]	12.3	23.3
2nd Overshoot [deg]	19.5	3.45
Yaw Check [s]	3.40	2.11
Reach [s]	11.8	10.9
Cycle Time [s]	22.6	17.5

The data, when compared to speed does follow a trend, but shows more scatter than the turning circle parameters. Each is plotted below in Figures 6.7 to 6.12 with respect to speed and desired angle. GPS track plots of the zig-zags can be found in Appendix C.

Note that the 8 knot, 10^0 case is not reported in the speed dependant plots below as initial attempts at these comparisons yielded outliers in all plots for this test case. The GPS plot shows the helmsmen had difficulty maintaining the desired course for this set. The second zig-zag test conducted shows better results which may indicate operator experience sensitivity.

All parameters are higher for the 20° cases, as expected. More experiments at this angle would be preferred to indicate trends. The initial turning time vs. speed for the 10° case remains relatively constant, indicating that the vessel reacts to helm input quickly and responsively at all speeds. Both the rudder reversing angle and the

1st overshoot angle increase with speed, which corroborate the turning circle data in that turning radius simply increases with speed.

However, the 2nd overshoot angle seems to have a constant or downward trend to the curve. This seems to contradict the earlier result in that the vessel reacts faster to helm input where there is a pre-existing yaw rate on the vessel.

The reach of the vessel also does not appear to increase with speed. This indicates the manoeuvrability from a time-domain point of view remains constant as the vessel increases speed. Interestingly, the cycle time, which is effectively two successive reaches, indicates a decrease in time to complete the manouver at increased speed.

All this tends to indicate a high manoeuvrability and quick reaction of the vessel at all speeds, with indications of increased manoeuvrability at higher speeds.

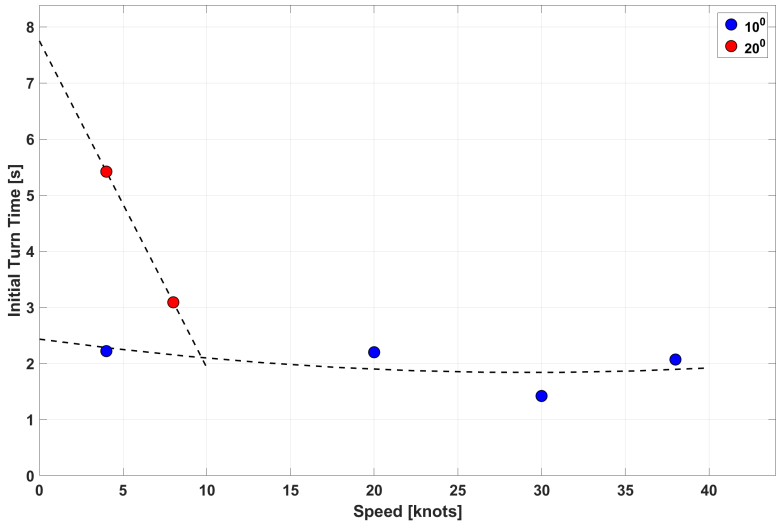

Figure 6.7: Initial Turning Time vs. Speed

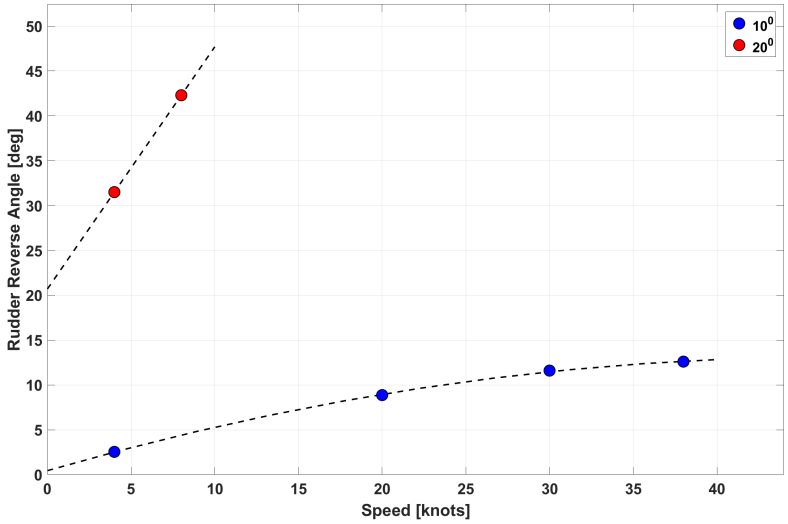

Figure 6.8: Rudder Reverse Angle vs. Speed

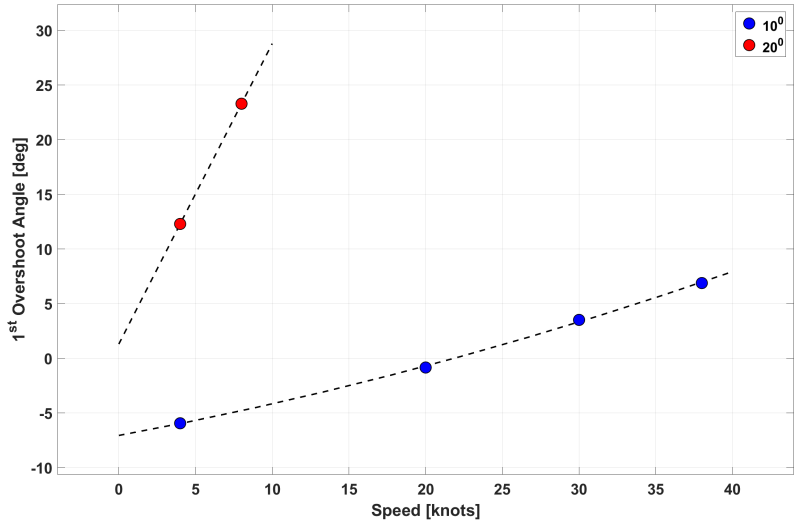

Figure 6.9: 1st Overshoot Angle vs. Speed

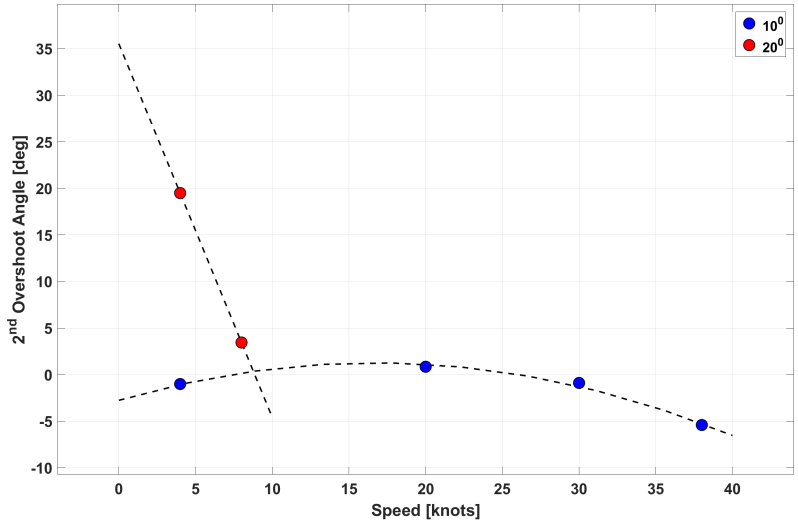

Figure 6.10: 2nd Overshoot Angle vs. Speed

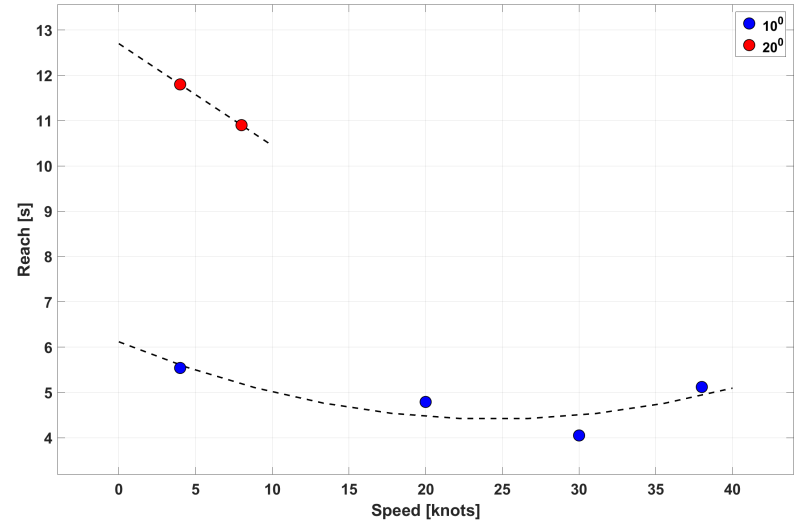

Figure 6.11: Reach vs. Speed

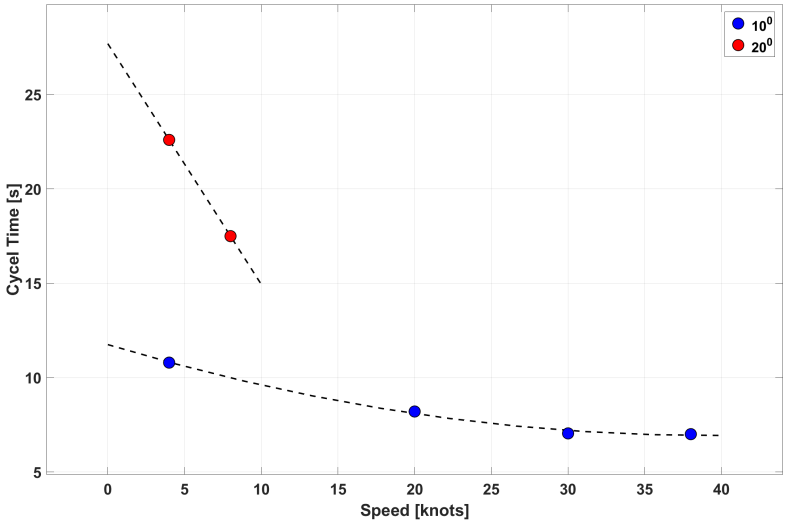

Figure 6.12: Cycle Time vs. Speed

6.4 Acceleration

There were two standing starts and five rolling starts, each starting at 4, 8, and 20 knots. These tests were completed upwind and downwind, which showed no discernible difference. Deceleration was also analysed following each standing start test.

The vessel slows rapidly initially but then its rate of deceleration decreases with speed. Near 4 knots, the stern wave catches the vessel and pushes it slightly, causing a temporary acceleration. As such, 4 knots was selected as the threshold for the end of the deceleration phase.

Plots of all starts are shown in Figure 6.13. It is clear that upon application of the throttle, the vessel follows nearly the same acceleration curve.

A summary of the standing start tests can be seen in Table 6.5. The vessel can

achieve maximum speed in under 20 seconds and takes about 250 metres to do so. The vessel stops in about two thirds of the time and 40% the distance.

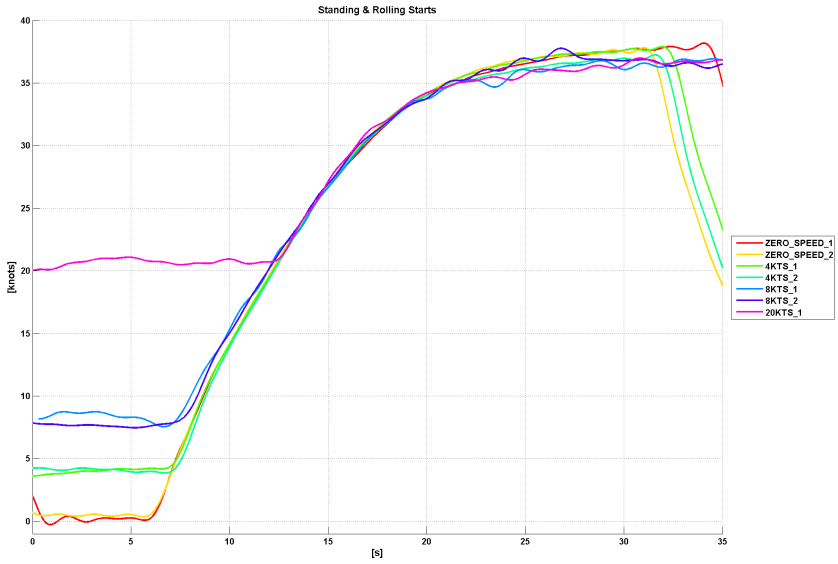

Figure 6.13: Standing and Rolling Start Test Results

Table 6.5: Acceleration Tests Results

Initial Speed	**Time to Max Speed [s]**	**Distance to Max [m]**	**Time to Stop [s]**	**Distance to Stop [m]**
0 knots	18.43	279.78	8.89	109.31
4 knots	16.20	234.10	8.00	79.12
8 knots	16.34	244.67	11.43	105.84
20 knots	14.06	222.30	12.35	119.59
Average	16.26	245.21	10.17	103.47

6.5 Towing

The results for the zero speed bollard pull are illustrated in Figure 6.14. The test was completed up to approximately 10 kN, similar to that experienced during a typical towing scenario. This maximum tow force was reached at an engine speed of around 2,600 rpm. The data fits a second order curve, as expected.

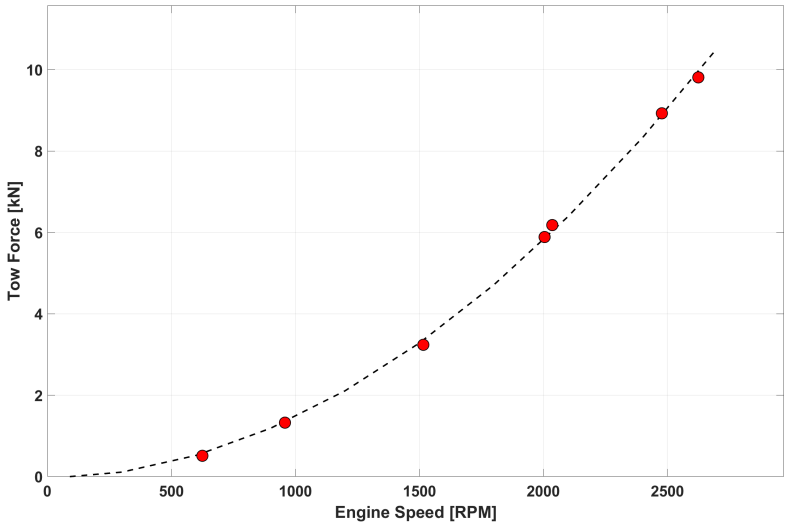

Figure 6.14: Tow Force vs. Engine Speed

A similar setup was used during the towing of the *Roberts Sisters II*. The generated tow force and achieved speeds are detailed in Figures 6.15 and 6.16. The curves shows more scatter, but trends as expected. Efforts to understand the source of this scatter were unsuccessful.

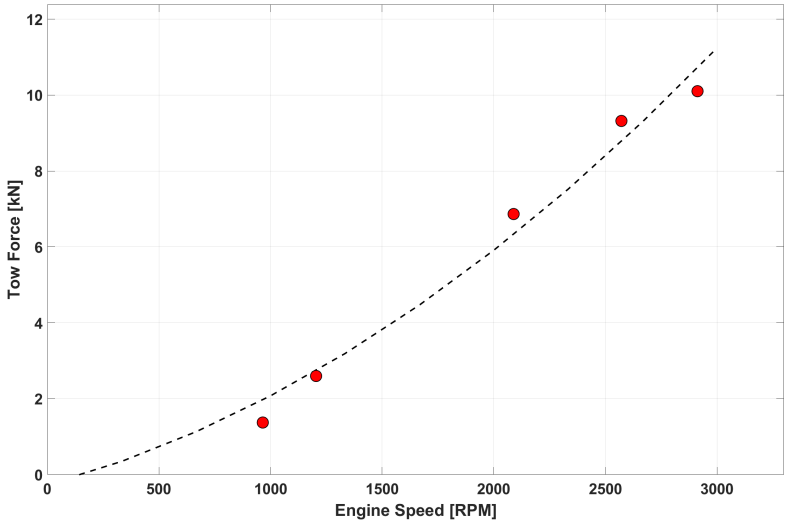

Figure 6.15: Tow Force vs. Engine Speed

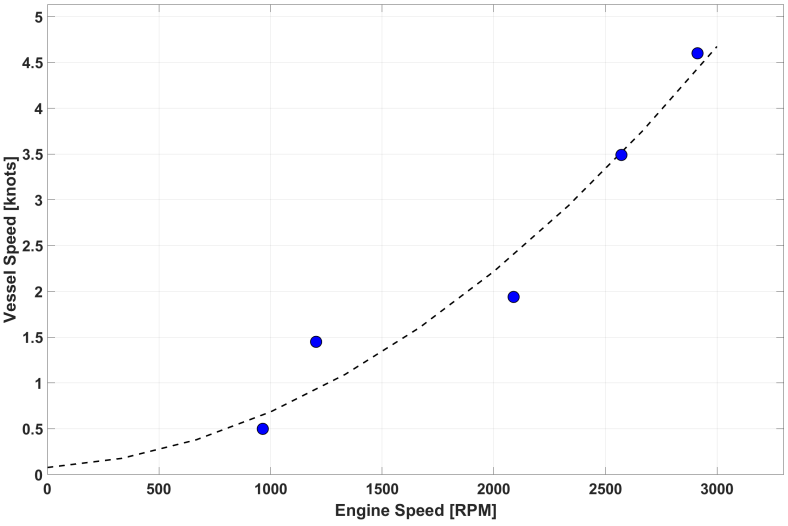

Figure 6.16: Achieved Speed vs. Engine Speed

As the fuel range of an FRC with a vessel under tow is of significant tactical value, the fuel consumption (litres per nautical mile) per segment was calculated. Based on full fuel tanks, the maximum range for the FRC when towing is extrapolated. The resultant curve can be seen in Figure 6.17

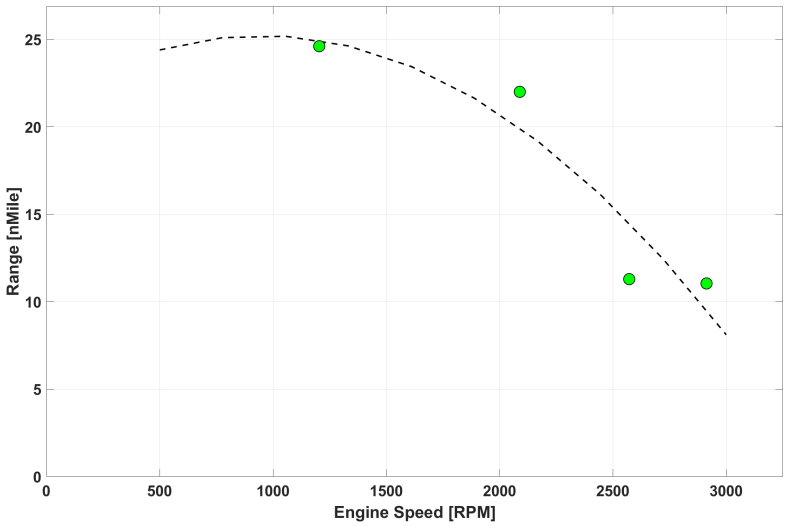

Figure 6.17: Vessel Range vs. Engine Speed

6.6 Star Patterns

The data is explored here in polar plots as discussed in Section 5.3.3.3. The three sections explored are: the helmsmen's difficulty to maintain heading, the difficulty of maintaining speed, and vessel motions. Each polar plot contains data for all headings and all speeds, and the various waves are shown on separate plots. A summary of the observed wave conditions is detailed in Table 6.6. The standard deviation of the

respective channel is used on the radial axis for all plots.

Table 6.6: Wave Conditions

Wave Condition	**Hs (metres)**	**Tp (seconds)**
1	0.40	6.51
2	0.52	2.71
3	3.60	11.90

6.6.1 Heading

The ability to maintain heading is assessed by examining the standard deviation of the course relative to wave and steering angle channels. A higher value on these indicates more variation and thus more difficulty maintaining course. Figures 6.18 to 6.20 outline the results for all headings with the steering angle on the left and the vessel heading on the right. The three waves are split between each figure.

The deviation of heading does reasonably mirror the deviation of steering input. Wave height is the most correlated parameter. The radius of each circle increases throughout each plot.

A large deviation occurred during the full speed test, which was only completed at the lowest wave condition. This shows that the largest difficulty to maintain heading occurred when the waves were coming from the starboard bow. The 30 knot case also appears to have more difficulty in this direction from this wave condition as well.

It is difficult to discern a speed trend during the lowest wave condition (apart from full speed), but the trend is more apparent for the two higher wave conditions.

It is observed that higher speeds actually show a better ability to maintain heading. This indicates that the vessel becomes more directionally stable at higher speeds.

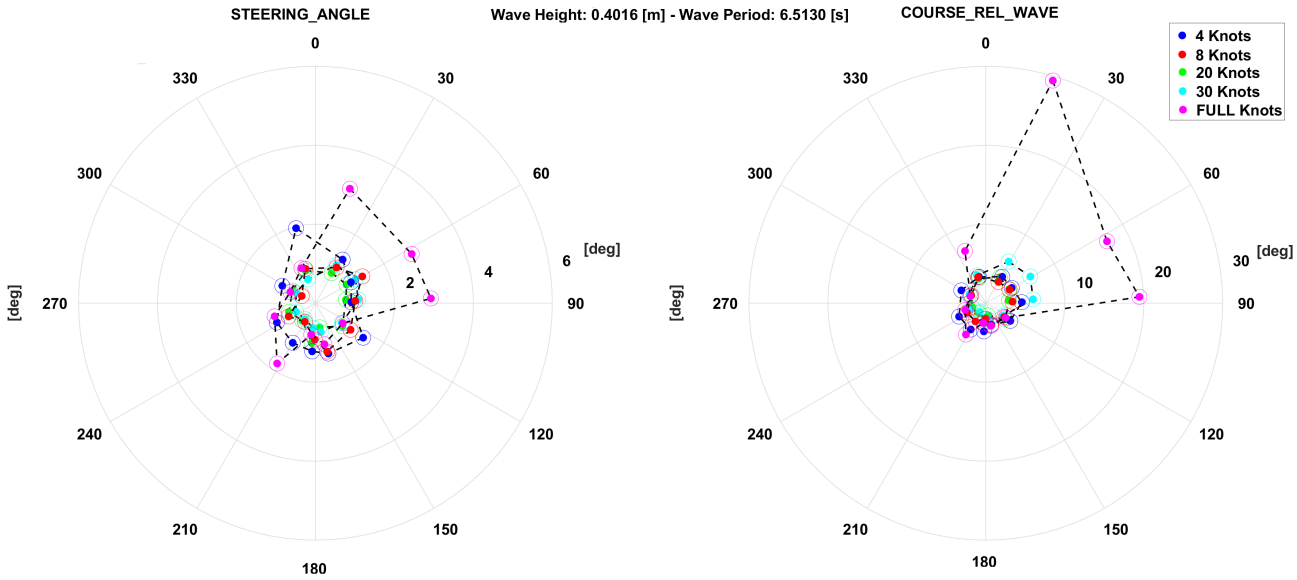

Figure 6.18: Ability to Maintain Heading - Wave Condition 1

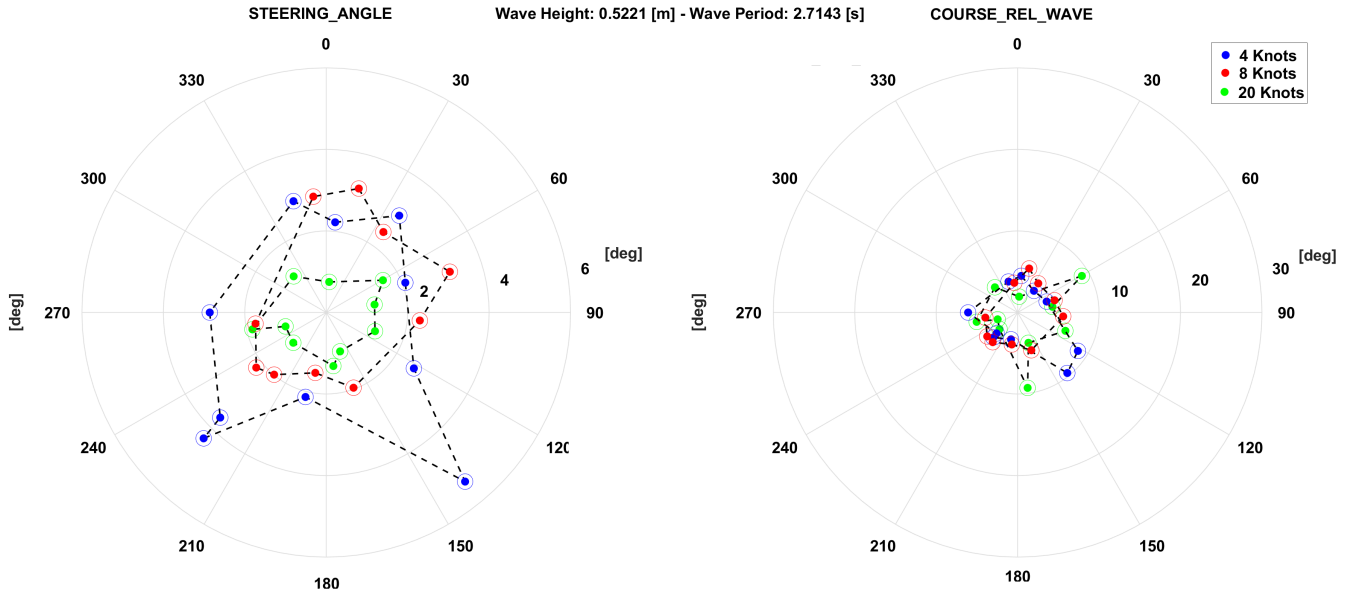

Figure 6.19: Ability to Maintain Heading - Wave Condition 2

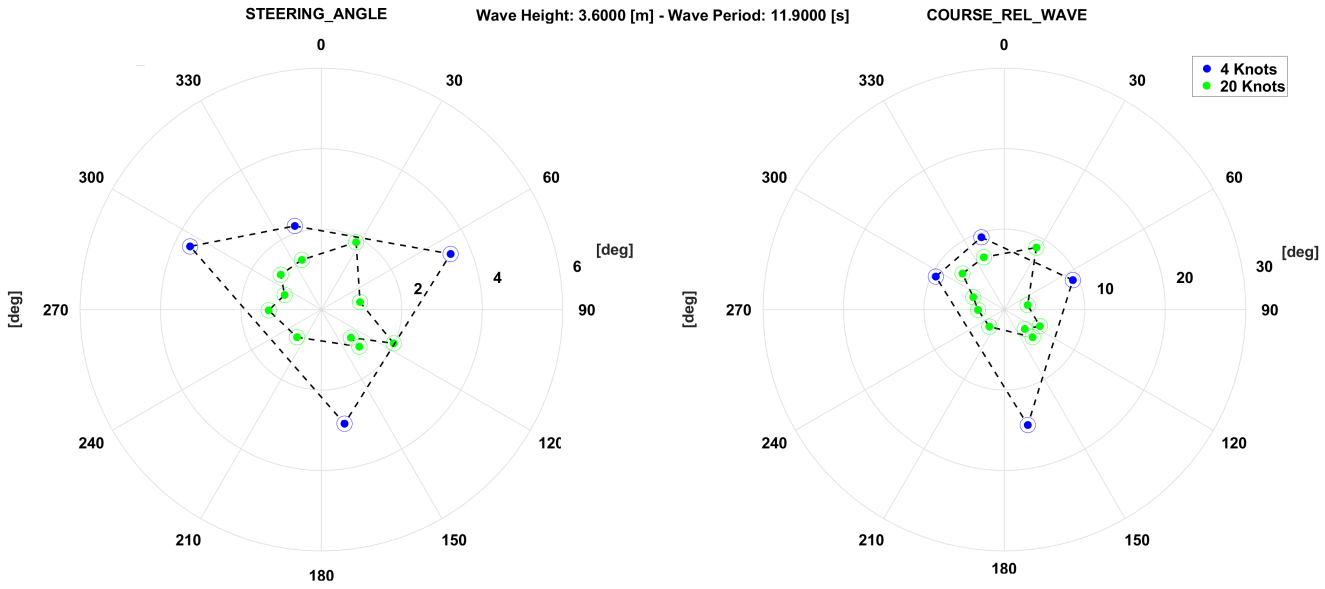

Figure 6.20: Ability to Maintain Heading - Wave Condition 3

6.6.2 Speed

Next, the ability to maintain speed was assessed by examining the engine speed and the achieved speed. Figures 6.21 to 6.23 outline the results similar to the previous section. The engine speed is on the left, and the achieved speed is on the right.

As with heading, the two chosen parameters do mirror each other well. The deviations also show a good correlation with increasing wave height.

There does not appear to be any prominent outliers as was seen when looking at heading. For the smallest wave condition, the desired speed does not appear to be a factor in ability to maintain said speed. However, both of the higher wave conditions indicate an increased difficulty in maintaining a set speed at higher desired speeds.

At the highest wave condition, the 20 knot case is wider in the centre of the plot, indicating an increased difficulty to maintain speed in beam waves. This is the only case where ability to maintain speed is affected by wave direction.

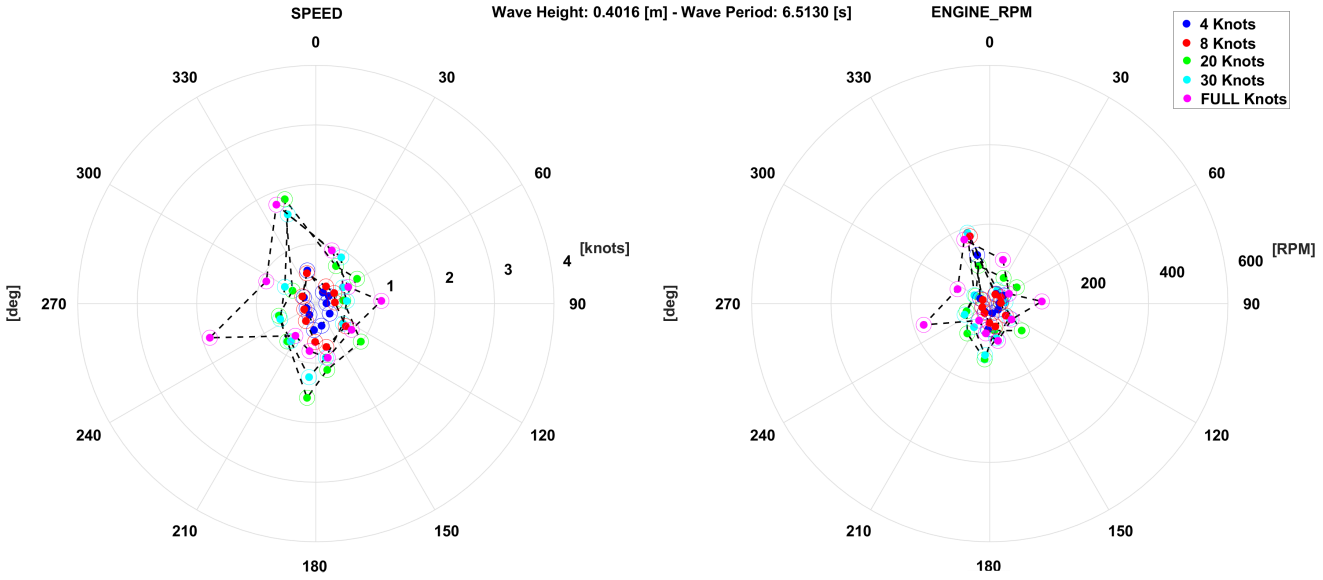

Figure 6.21: Ability to Maintain Speed - Wave Condition 1

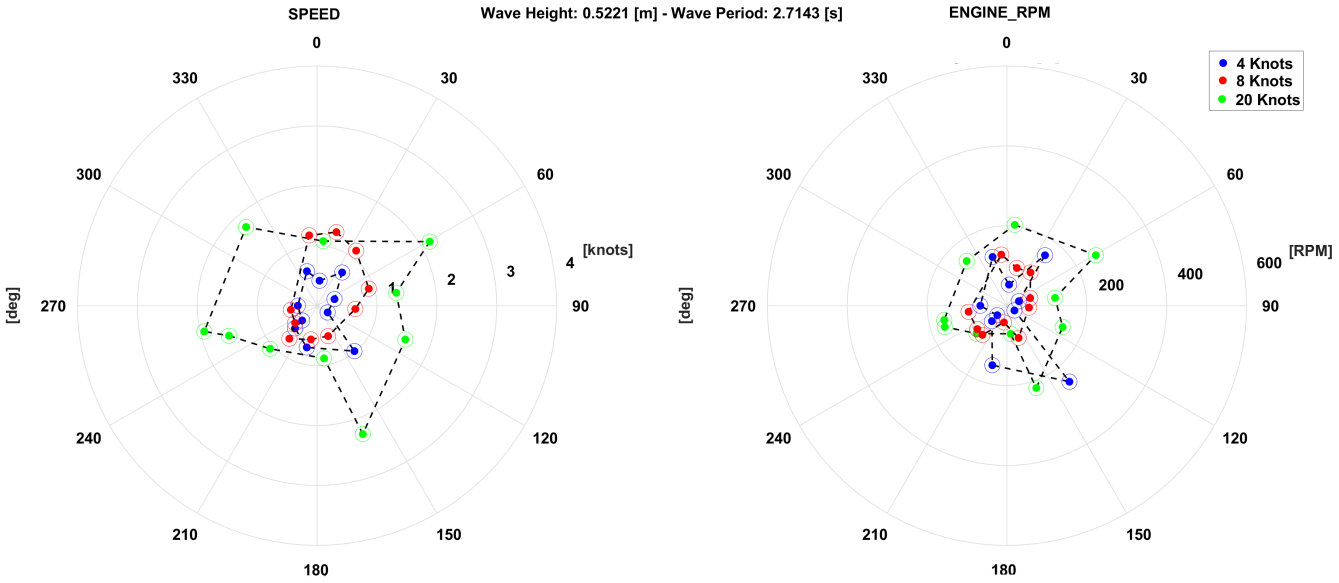

Figure 6.22: Ability to Maintain Speed - Wave Condition 2

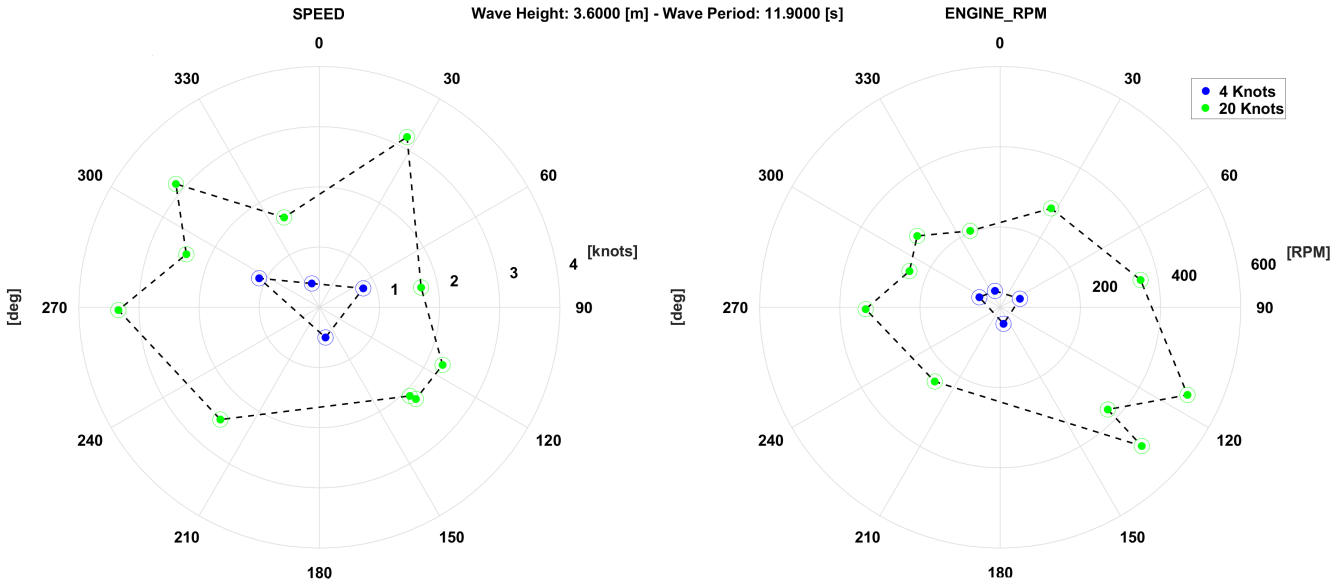

Figure 6.23: Ability to Maintain Speed - Wave Condition 3

6.6.3 Vessel Motions

The standard deviations of roll, pitch, and Z-acceleration are observed in a similar manner as speed and heading. The Z-acceleration is presented separately from the pitch and roll.

6.6.3.1 Z-acceleration

Figures 6.24 to 6.26 show the polar plots for Z-acceleration. It is very clear from the first wave that the standard deviation of Z-acceleration directly correlates with increasing speed. The deviations increases incrementally as the speed increases. This trend is shown on the wave condition 2 and wave condition 3 plots as well. The increased wave height also correlates with the Z-acceleration as expected if one follows the trends of similar speed throughout the plots.

At the lowest wave condition, direction does not seem to affect the acceleration deviations. During the second wave, following seas tend to show much more deviation in Z-acceleration than head seas. The third wave indicates higher deviations when waves are coming from starboard.

It is also noteworthy that the maximum Z-acceleration experienced by the vessel throughout testing was 4.67 times gravity. As a reminder, the Z-acceleration is reported about a location in the pilot's console. The crew does have shock-absorbing seats, however. Accelerations on the bodies of the crew were not measured, although this may be of interest in future research.

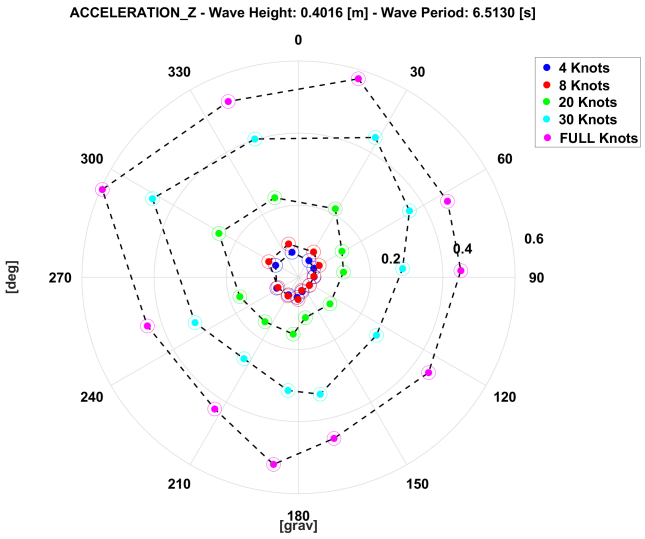

Figure 6.24: Z-acceleration - Wave Condition 1

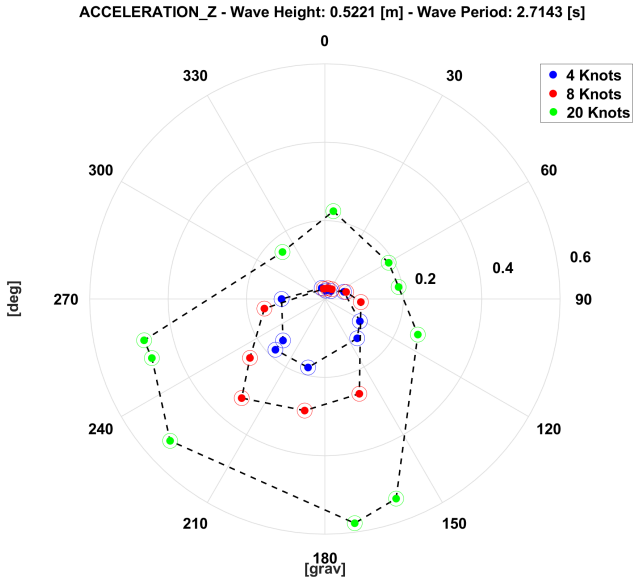

Figure 6.25: Z-acceleration - Wave Condition 2

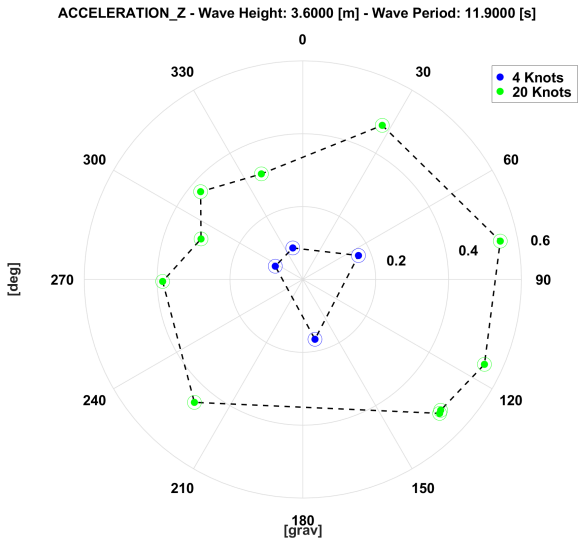

Figure 6.26: Z-acceleration - Wave Condition 3

6.6.3.2 Pitch and Roll

Figures 6.27 to 6.29 show the polar plots for both pitch and roll for all wave heights.

The standard deviation in pitch does increase with speed for all wave types whereas the roll does not seem to follow a discernible trend when compared to speed. Both of these tendencies are expected as the encounter frequency in the forward direction changes with speed, but not in the beam-on direction.

The wave height has a pronounced effect on the motions, increasing the standard deviations in both pitch and roll. The direction does not appear to have an effect on the pitch motions for any wave. The roll motions at the lowest wave do not seem to be direction dependant, but direction has a pronounced effect on roll on the second wave. The beam-on waves show an increase in the standard deviations between 3

or 4 times. This trend is also observed at the highest wave, but the increase due to direction is only slight. That being said, the motions are already extreme in all directions and may hint to secondary stability of the vessel [14].

Throughout the data set, the maximum pitch experienced by the vessel was 24.8° bow up and 11° bow down. The maximum roll experienced was 22.5° starboard down, which is similar to the measurement of to 21.4° port down.

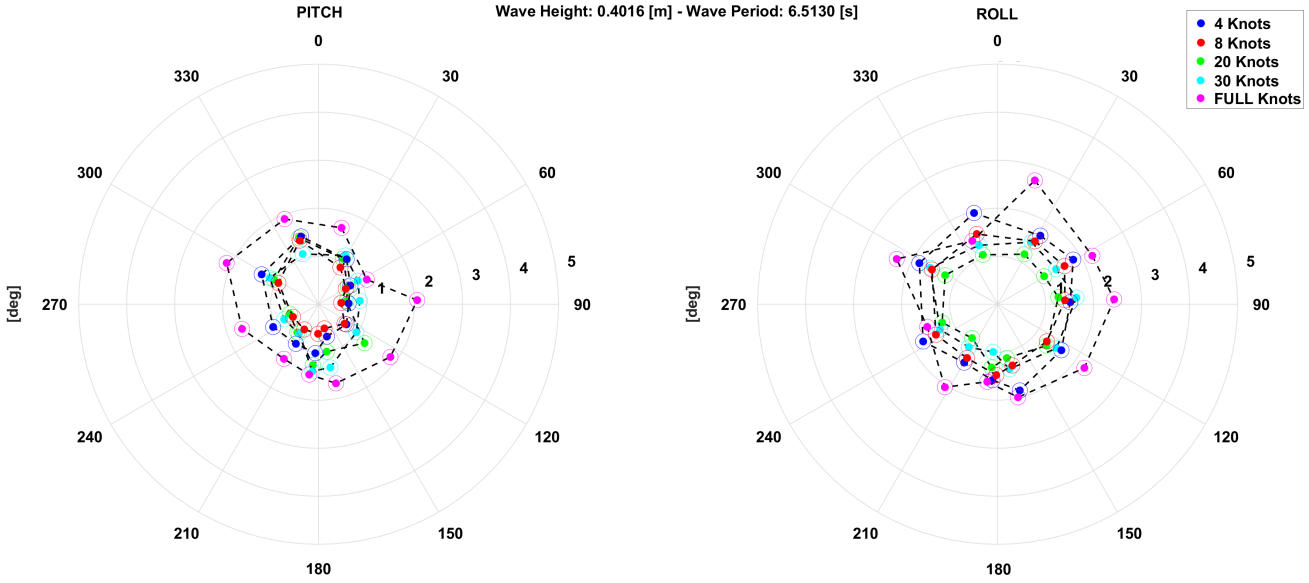

Figure 6.27: Pitch and Roll - Wave Condition 1

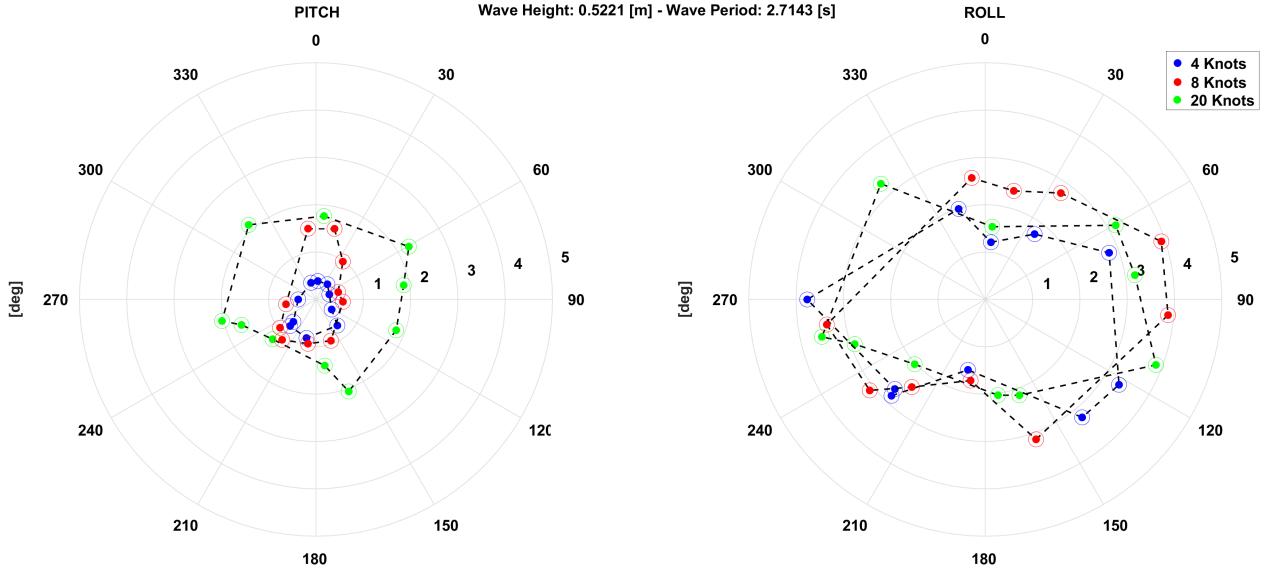

Figure 6.28: Pitch and Roll - Wave Condition 2

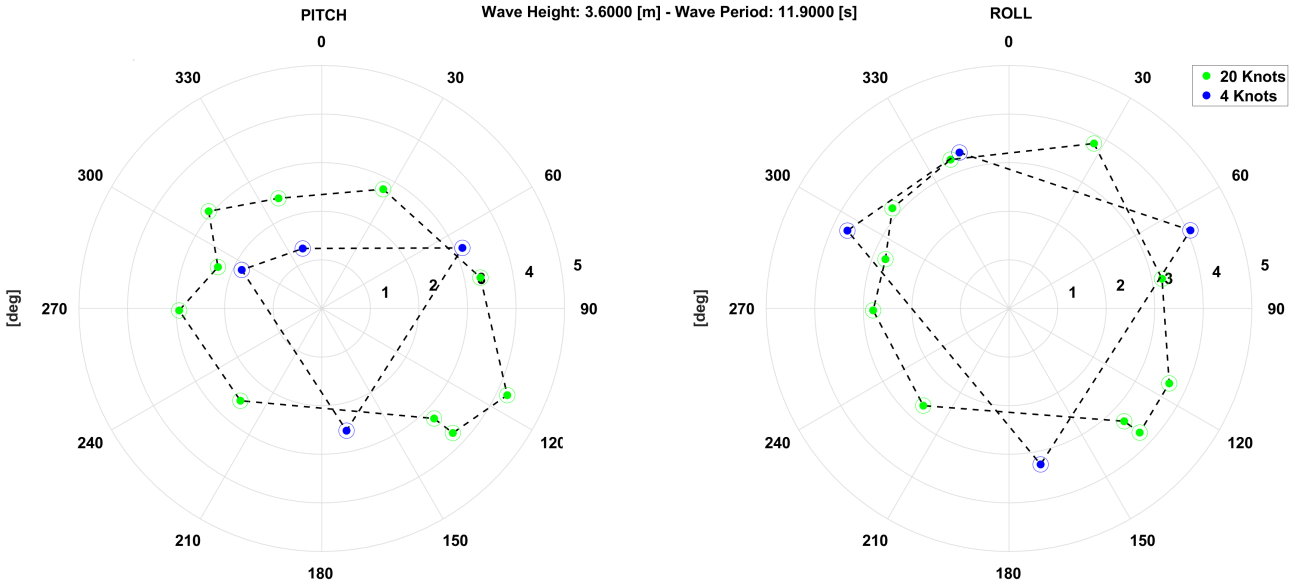

Figure 6.29: Pitch and Roll - Wave Condition 3

6.7 Performance Curves

As per the analysis procedures outlined in Section 6.7, various correlations between channels are outlined in the following sub sections. All data presented here has undergone the sub segmentation data reduction method as discussed in Section 5.3.4.2.

6.7.1 Engine Performance

To asses the performance of the engines, the engine speed was plotted against the fuel consumption for each engine, as can be seen in Figure 6.30.

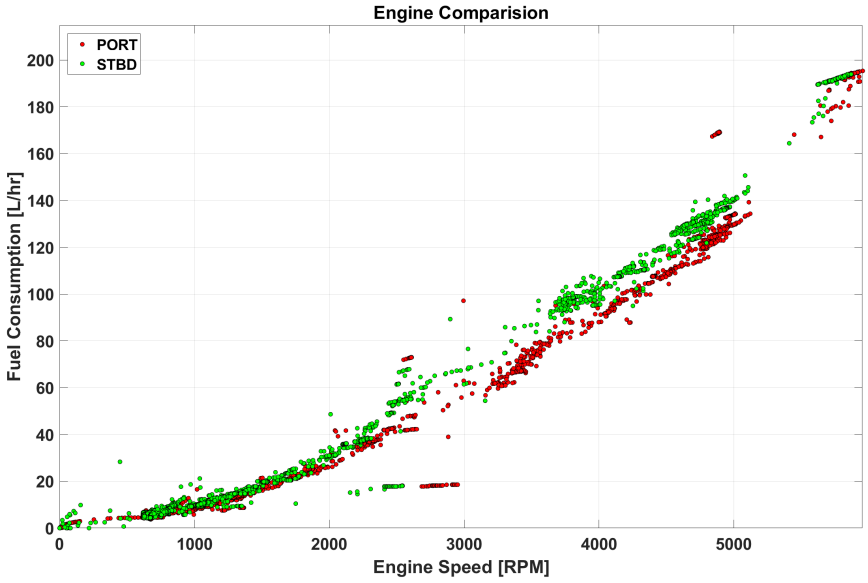

Figure 6.30: Engine Comparison, All Data Points

From this comparison, there are two anomalies present. First, there are data points between 2000 and 3000 rpm which show relatively low fuel consumption. The

data points were indexed and plotted on the time series, as seen in Figure 6.31.

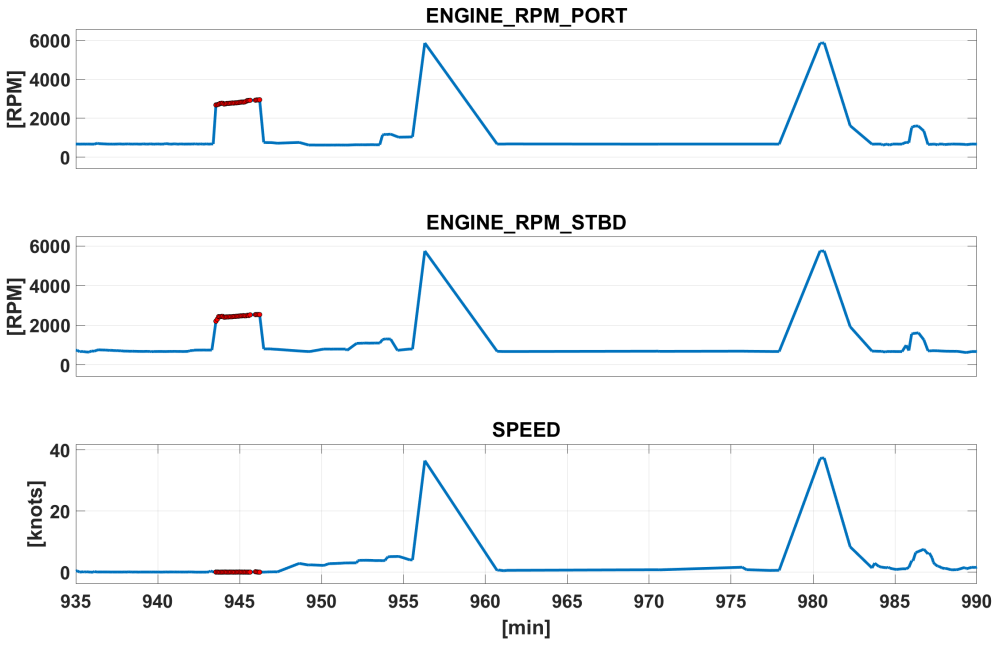

Figure 6.31: Low Fuel-High rpm

From here it can be seen that the vessel speed for these data points is actually 0 knots. The location from the latitude and longitude also indicate that the vessel is docked in port. As such, it is presumed that these data points are from an attempt to "warm up" the engines by revving the engines at high rpm with no load, which yielding a low fuel consumption. These data points were thus removed from the performance curves.

There is also another anomaly occurring at 4850 rpm, where the port engine shows high fuel consumption relative to its rpm. Similarly, by inspection of the time series as above, the cause is determined in Figure 6.32.

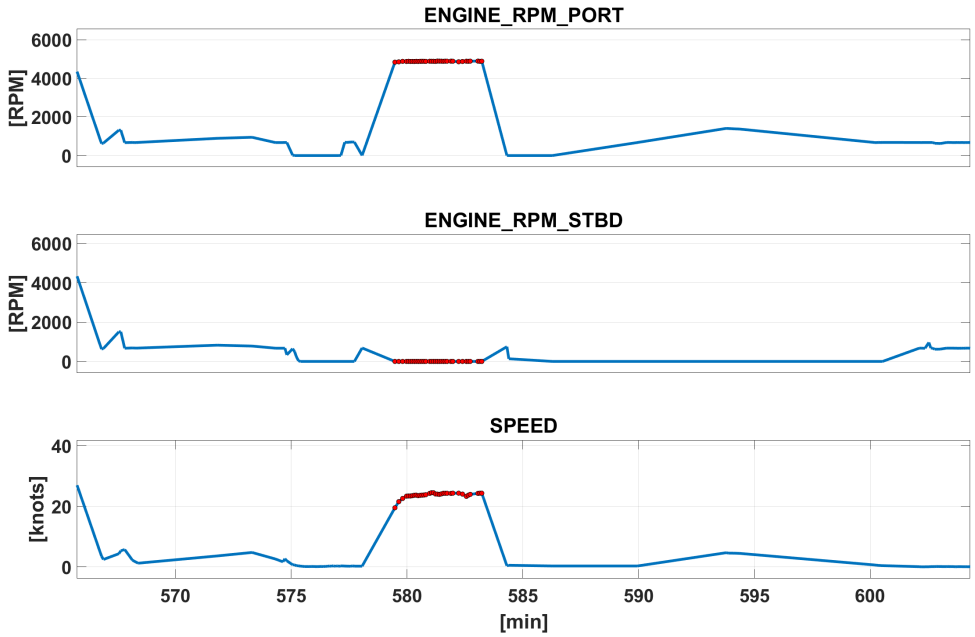

Figure 6.32: High Fuel-Low rpm

As shown in the figure, this was caused by only a single engine functioning. Referencing the test logs, there was an instance where the port engine failed and the vessel returned to port on the starboard engine only. These data points were removed to yield an engine performance curve as can be seen in Figure 6.33.

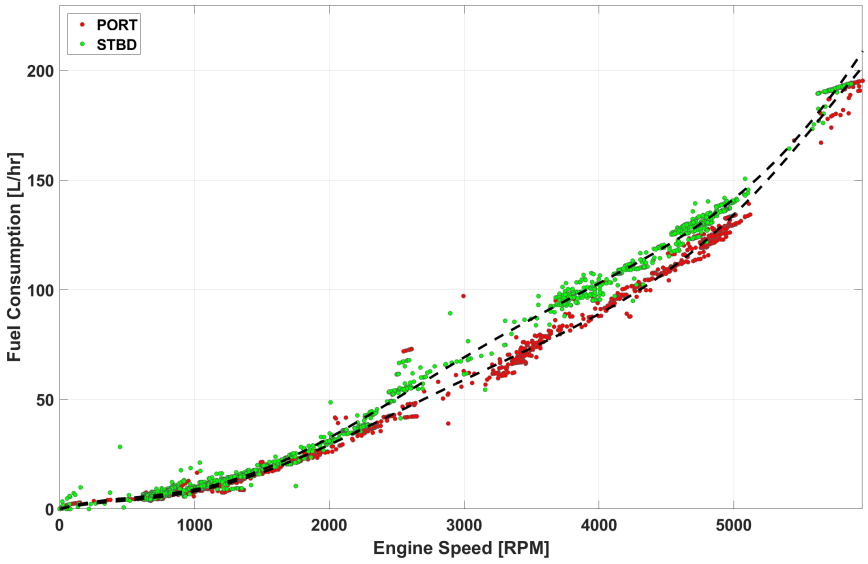

Figure 6.33: Engine Comparison Final

It can be also seen from Figure 6.33 that the starboard engine is underperforming the port in terms of fuel consumption. While the source of this discrepancy is unknown, it can be quantified. Figure 6.34 compares the percentage difference between the two engines. While the difference varies, the starboard engine is approximately 10% less efficient than the port around the operating range of the engines.

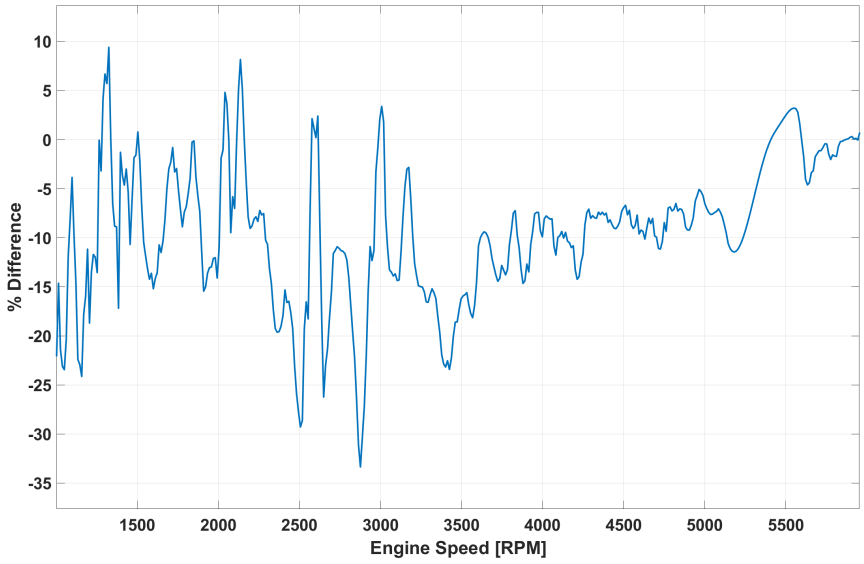

Figure 6.34: Engine Comparison - % Difference

Finally, the occurrence where a single engine was used was analysed to determine the effect of fuel efficiency on single engine use. The average speed using one engine was 23.74 knots, yielding a fuel efficiency of 7.12 L/nautical mile. The closest occurrence of this speed with two functioning engines was 24.7 knots, which yielded a fuel efficiency of 7.99 L/nautical mile.

The duration of this examined data is 4.25 minutes over 1.8 nautical miles. To best determine the effect of single engine use, a set of data over the full operating range of the vessel would be advised. It is also noteworthy that a single engine vessel, which may be more efficient for this speed, would not have the security of redundant engine setup. Nor would it achieve the speed, acceleration, or towing capabilities of the two-engine craft.

6.7.2 Fuel Consumption

Next, fuel consumption vs. speed was plotted. Figure 6.35 outlines this curve for both engines and the summation of the two.

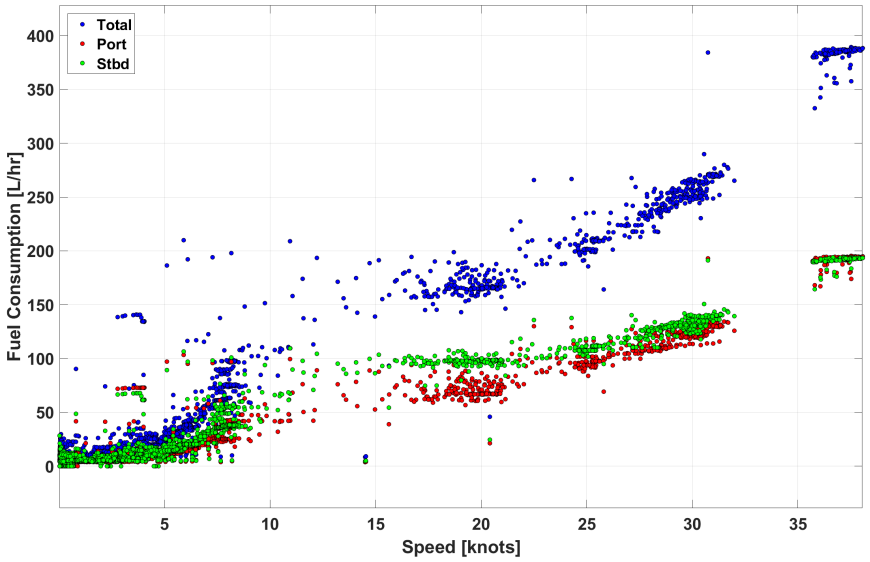

Figure 6.35: Fuel Consumption vs. Speed

As before, there were anomalies to investigate. There are high fuel consumption values below 5 knots shown on both engines. Plotting the location (based on the time of this occurrence) shows that these data points were acquired during the towing experiment outlined in Section 4.4.2. These data points were thus removed.

Next, to better asses the spread of data, the total fuel consumption data was plotted against wind direction, separated into three bins: beam wind, head wind, and tail wind as in Figure 6.36. From this plot, it is observed that there is very

minimal effect of wind direction on fuel consumption.

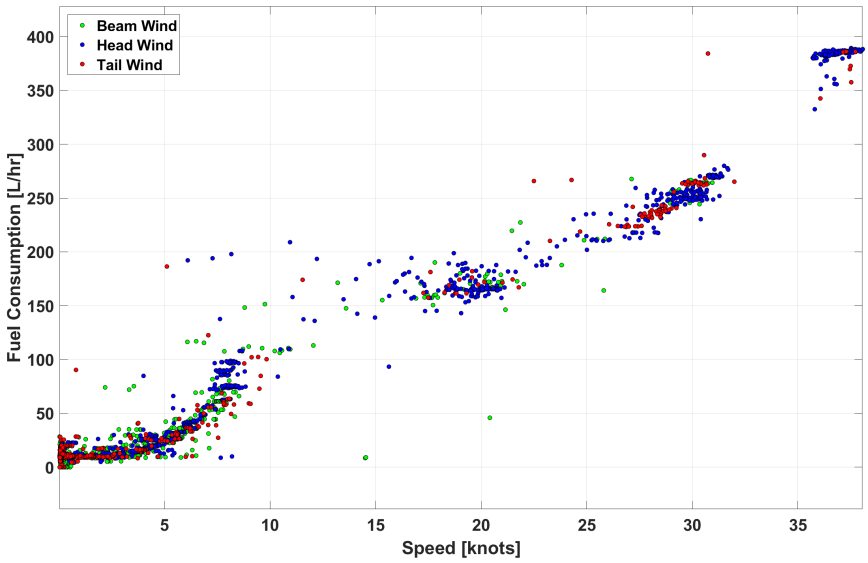

Figure 6.36: Fuel Consumption vs. Speed vs. Wind Direction

The apparent wind speed is similarly compared in Figure 6.37. The wind speed steadily increases with speed with little variation in the trend. As with the direction, the wind speed appears to have minimal effect as well, save for the portion of data surrounding 20 knots.

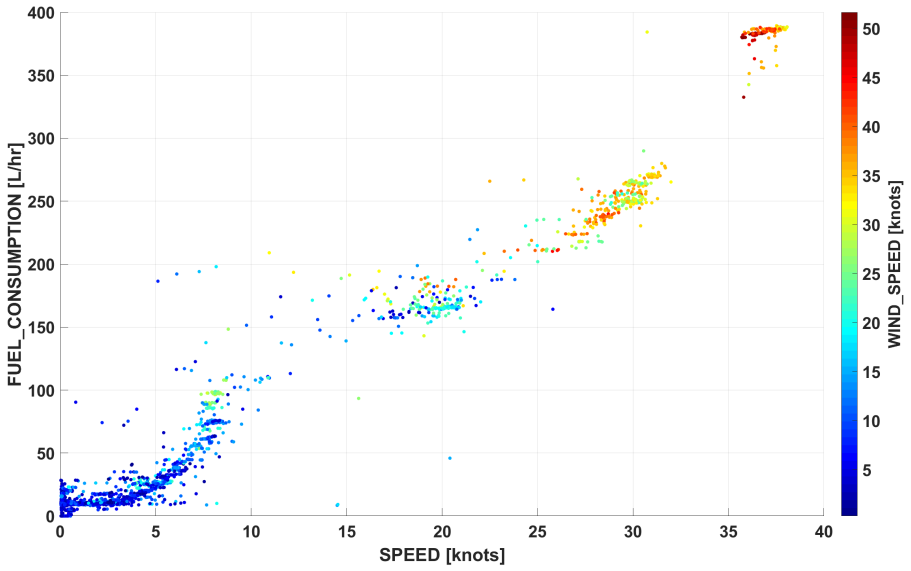

Figure 6.37: Fuel Consumption vs. Speed vs. Wind Speed

Finally, wave height is considered in Figure 6.38. The wave height is grouped into three bins: less than 0.5 metres, between 0.5 metres and 1.5 metres, and finally above 1.5m. Note that the highest wave condition is not tested at high speeds, and thus its effect on fuel efficiency cannot be assessed. However, the two lower clusters of wave height are intermingled, also indicating minimal effect on fuel efficiency.

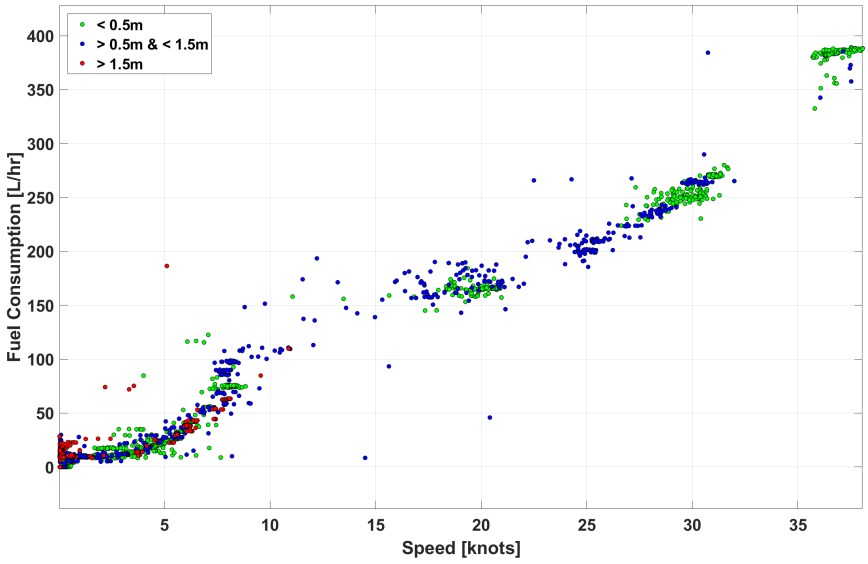

Figure 6.38: Fuel Consumption vs. Speed vs. Wave Height

As such, the data is plotted and a trend line is fitted as in Figure 6.39. The fitted curve is a fifth order polynomial. The coefficients identified on the graph follow the general form of Equation 6.1, where S is speed in knots, and Y is the fuel consumption in litres per hour.

The three distinct phases of planing hulls are also clear on this plot. The typical Froude resistance curve is observed up to approximately 9 knots. The transition zone is between 9 and 17 knots. Beyond this, the planing resistance curve is observed up to the maximum speed. The end of the transition zone is observed very close to Savitsky's prediction of 17.4 knots based on a Froude Number of 1.0 [20].

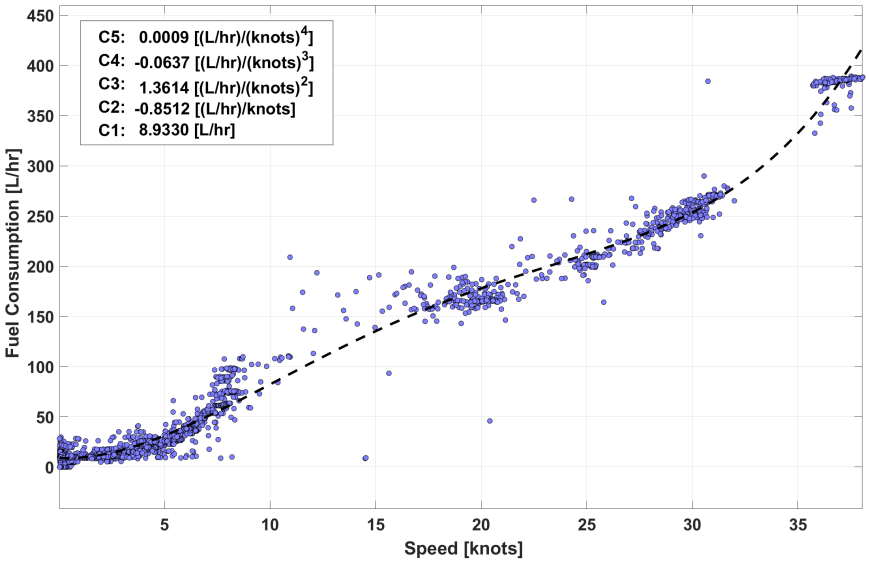

Figure 6.39: Fuel Consumption vs. Speed vs. Wave Height

$$Y = C_1 + C_2(S) + C_3(S)^2 + C_4(S)^3 + C_5(S)^4 \tag{6.1}$$

From an operational point of view, it is also useful to know the engine speed required to achieve a desired speed. The average engine speed for each data point is plotted against the achieved speed in Figure 6.40.

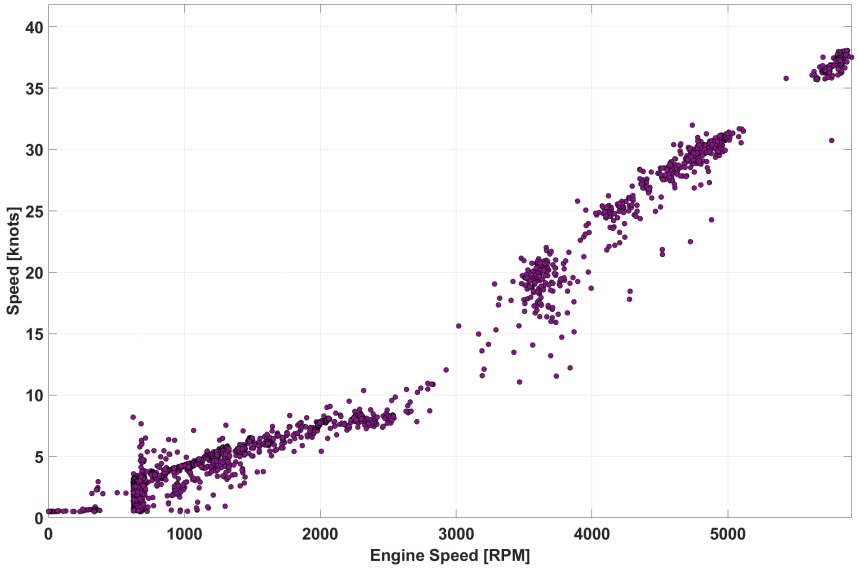

Figure 6.40: Engine Speed vs. Speed

6.7.3 Fuel Efficiency

Next, fuel efficiency is examined to yield operational metrics. The fuel consumption is divided by the speed to calculate a L/nautical mile channel. This is then plotted against the speed, generating the plot in Figure 6.41.

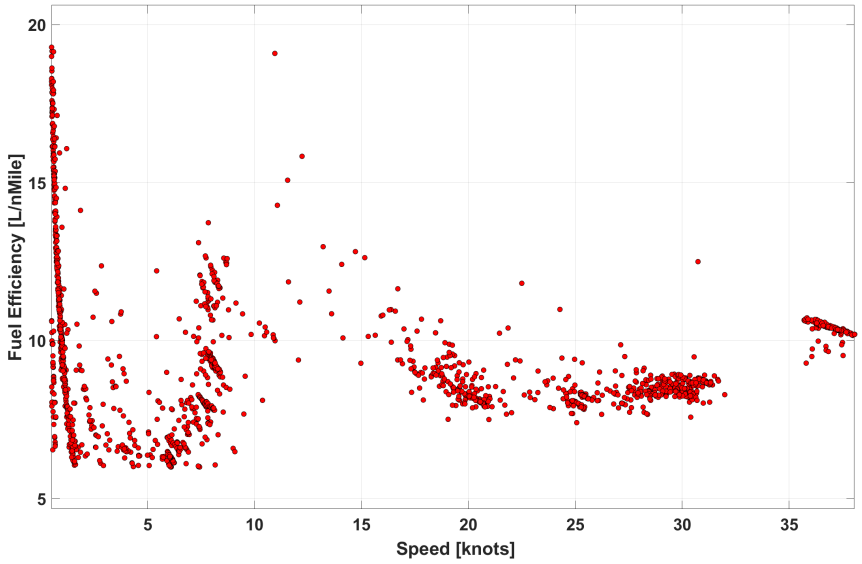

Figure 6.41: Fuel Efficiency vs. Speed

Finally, given the FRC's fuel capacity of approximately 450 litres, the range was calculated for each speed, generating the plot in Figure 6.42. A curve was fitted to the portion the of data above 10 knots, since operating below 10 knots is not practicable for a vessel of this mission profile. The fitted curve's coefficients follow the 5^{th} order polynomial in Equation 6.1, where Y is the range in nautical miles.

An interesting value is presented by this fitted curve. The maxima of the upper portion yields the most fuel efficient speed and associated range for this vessel. At a cruising speed of 24.6 knots, the vessel can achieve a range of 56 nautical miles based on its fuel carrying capacity.

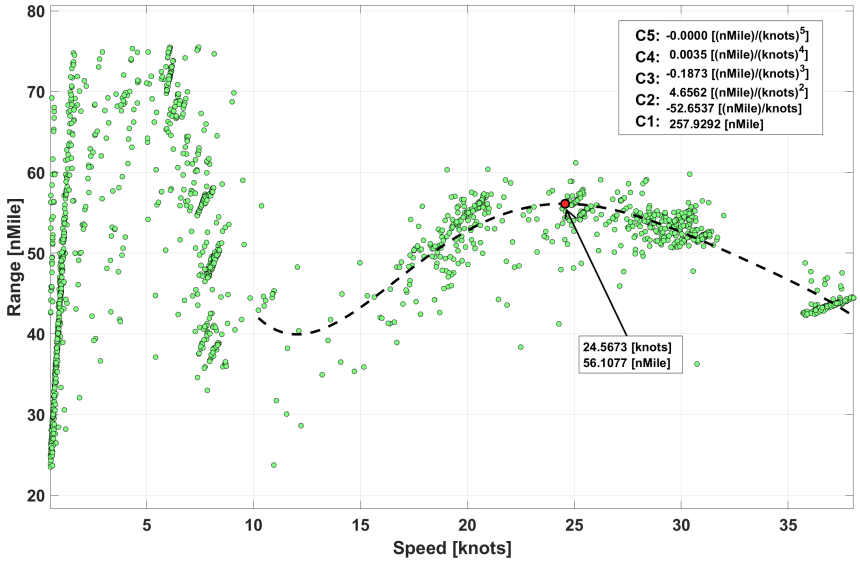

Figure 6.42: Range vs. Speed

6.7.4 Human Kinetics

Finally, to supplement Section 6.6, the effect of speed and wave height on accelerations, angular rates, and steering angles was explored. This analysis considers the entire data set of collected data, whereas Section 6.6 only considers certain legs of the star patterns.

6.7.4.1 Accelerations

Figures 6.43 and 6.44 show the effect of speed and wave height on the standard deviation of accelerations in three directions. The speed shows higher maxima and range with increasing speed for all. The Z-acceleration is by far the most sensitive to

speed, followed by Y acceleration, and finally, X acceleration.

The hierarchy is similar when comparing wave height, however the spread is less discernible with increasing wave height, except for at the lower end.

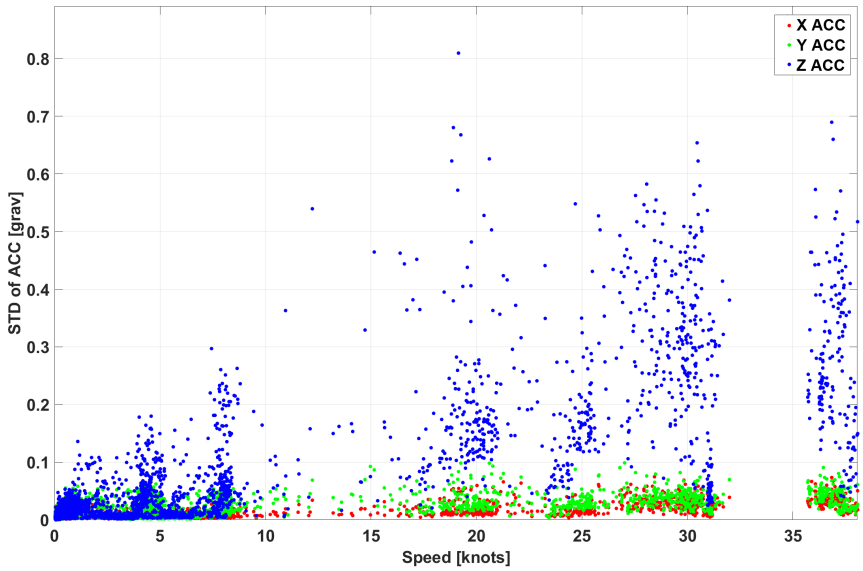

Figure 6.43: Standard Deviation of X, Y, and Z-acceleration vs. Speed

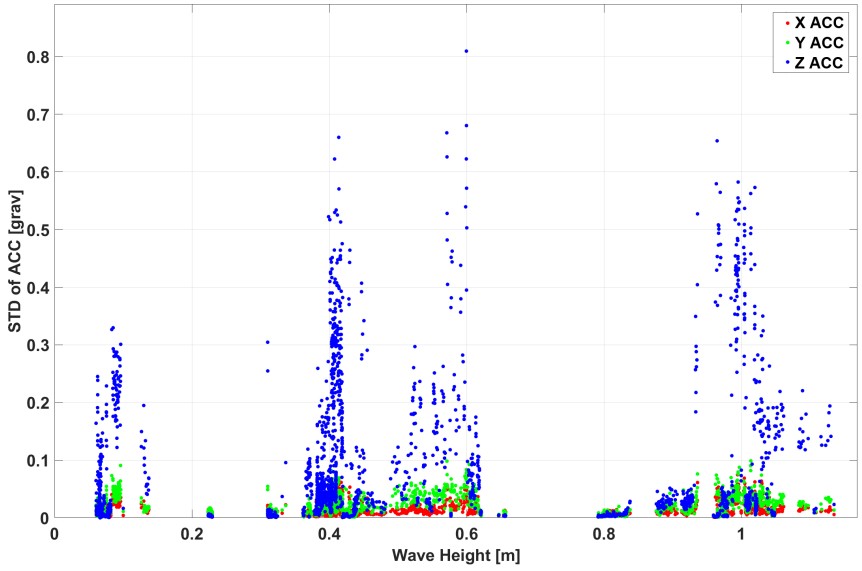

Figure 6.44: Standard Deviation of X, Y, and Z-acceleration vs. Wave Height

6.7.4.2 Pitch and Roll Accelerations

Figures 6.45 and 6.46 show the effect of speed and wave height on the standard deviation of roll and pitch rate. The ranges of the data have opposite trends when compared to speed. The roll rate decreases with speed, whereas the pitch rate increases. The reduction in roll rate can be attributed to dynamic stabilization of the planing hull [4]. The increase in pitch is expected due to increased slamming experienced at higher speeds.

The wave height's effect on the roll rate is similar to that of the accelerations. Much scatter is shown in the data apart from the low end which show lower values than the rest. The pitch, however, shows a curious lull in motion around the centre

of the wave height. This may be due to the period being well outside the natural frequency of pitch of the vessel. Further investigation into this phenomena would be advisable.

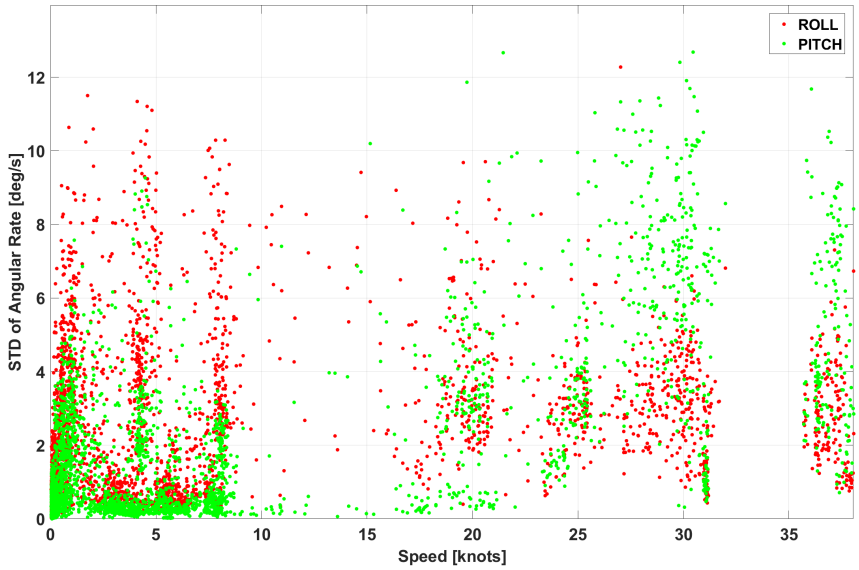

Figure 6.45: Standard Deviation of Roll and Pitch Rate vs. Speed

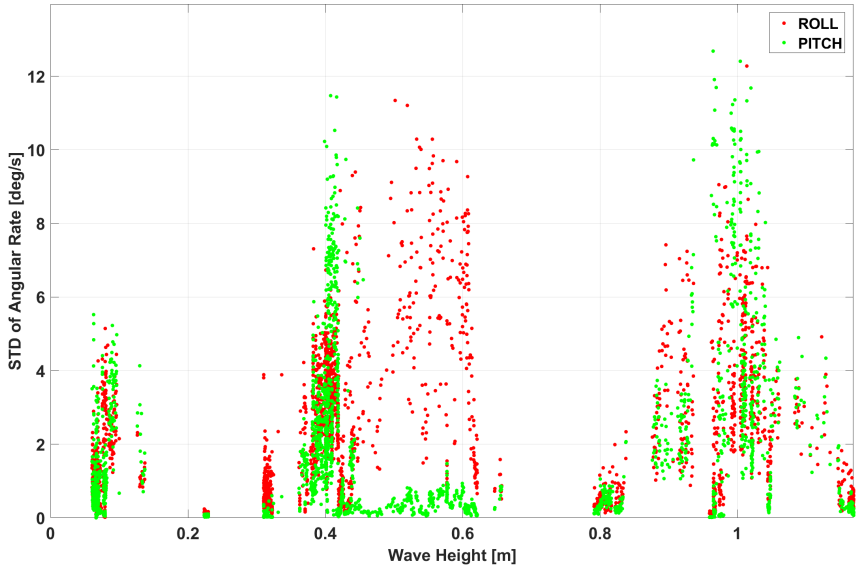

Figure 6.46: Standard Deviation of Roll and Pitch Rate vs. Wave Height

6.7.4.3 Steering Angle

And finally, to conclude the results section of this report, Figures 6.45 and 6.46 show the effect of speed and wave height on the standard deviation of steering angle. The data shows a prominent decrease in steering angle deviation with speed. This is likely caused by increased directional stability at higher speeds and possibly operator reluctance to varying helm input at higher speeds.

The wave height's effect is again curious, showing a higher spread in the middle range of wave height, lower range at the high end, and an ever lower range of helm input at low wave heights.

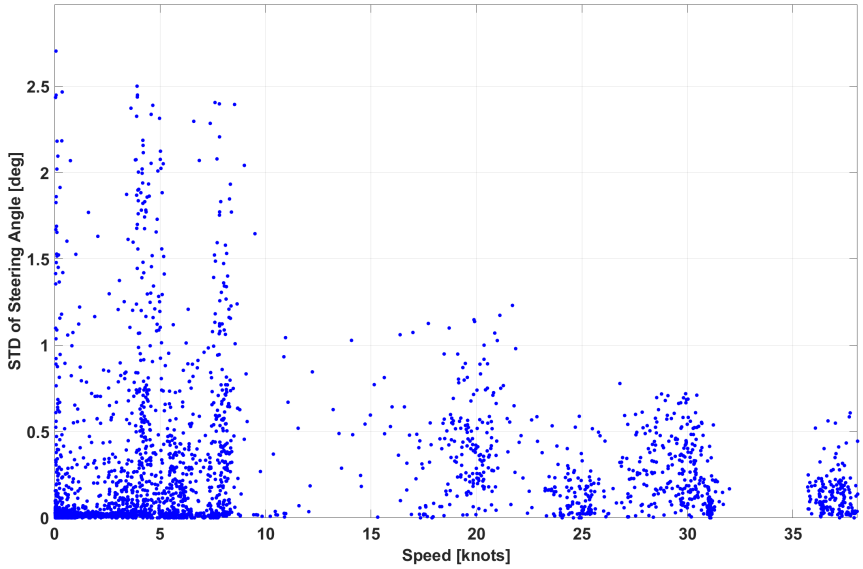

Figure 6.47: Standard Deviation of Steering Angle vs. Speed

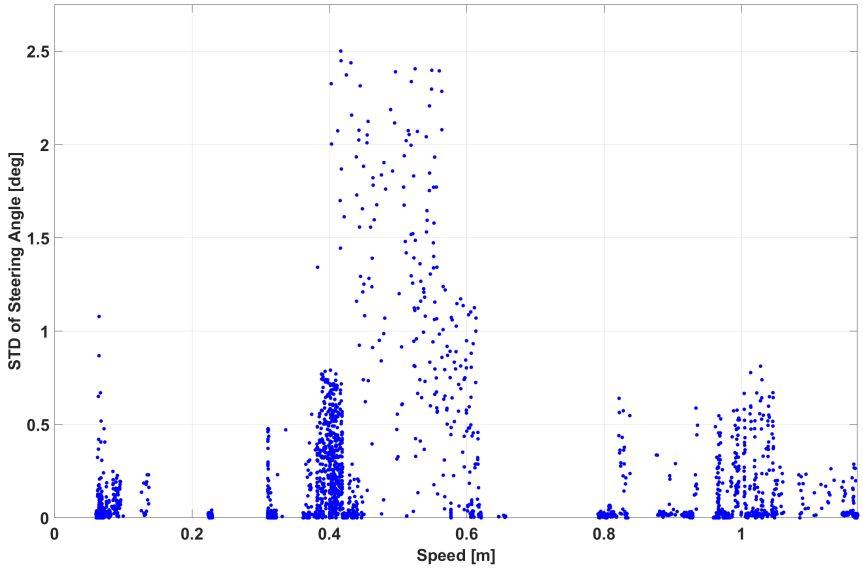

Figure 6.48: Standard Deviation of Steering Angle vs. Wave Height

Chapter 7

Conclusions

The efforts outlined in this experimental program yield a baseline for comparison in considering other crafts of this type. The results of the collected data have added insight into the areas of vessel performance, fuel economy, and human kinetics. The following sections outline key information attained in each area.

7.1 Vessel Performance

The vessel performance was assessed by completing a series of prescribed tests. The turning circles showed the vessel can execute a full about face turn in just over 200 metres at full speed and just under 20 metres at a manoeuvring speed. The zig-zag experiments show that the vessel is very reactive to helm input and can even show higher performance in time-dependent metrics at greater speeds. The vessel can reach its maximum speed in under 20 seconds and 250 metres, and its acceleration is independent of initial speed. Finally, the vessel has shown ability to tow a 19.7 metre fishing vessel at speeds up to 4.5 knots.

7.2 Fuel Economy

The engines do appear to perform asymmetrically, with the port engine out performing the starboard by about 10% over the operating range. The fuel economy is generally unaffected by wind speed, direction, or even wave height. The fuel consumption curve fits a typical planing craft resistance curve. Its maximum range of 56 nautical miles is achieved at its optimal cruising speed is 24.6 knots.

7.3 Human Kinetics

Accelerations in the Z direction are the most pronounced, followed by accelerations in the Y and finally X directions. The effect of speed is prominent in all three. Beam waves produce an increase in Y direction accelerations. The maximum Z acceleration recorded was 4.67 times gravity. The helmsman's ability to maintain heading is increased with speed due to the vessel becoming more directionally stable at higher speeds. Wave height has a prominent effect on the helmsman's ability as well.

Chapter 8

Recommendations

As this experimental program was intended as a baseline, further investigations into other similar craft would yield valuable comparative analyses. While other FRCs may have similar vessel performance, fuel efficiency of the propulsion units can also be assessed without the need to complete defined experiments. The sub segmentation analysis can be completed on any sufficiently large data set to populate the desired trends.

The curious lull in pitch motions during the middle range of the wave condition would be useful to investigate through further testing and observation.

Crew comfort could be studied in further detail with better instrumentation. Dynamics of the craft as a whole were observed, but the reactions of the crew from a motion induced interrupted, or motion sickness index could be explored. Instrumentation of the actual crew is also suggested for future work.

The GPS data at low speed has some discretization associated with the output. This may hint that the fidelity of the sensor may not be sufficiently high for low

speed manoeuvers. At higher speeds and extreme values, the sensor shows good resolution. This is to say, the most relevant portions of the data has sufficient quality for consideration.

While the acquisition system proved sufficiently reliable, there were some data dropouts throughout the program. Initial investigations into these points towards an unreliable alternator output from the engines. A buffering device, such as an uninterrupted power supply unit, could be used in future iterations of the acquisition system to yield higher reliability.

References

[1] Mackie, Rick "DSI - Reporting for Duty! | Mercury Racing," *Mercury Racing*, 19 May 2015, 8 Aug. 2016 <http://www.mercuryracing.com/optimax-diesel-reporting-for-duty/>

[2] Fridsma, Gerard "A Systematic Study of the Rough-Water Performance of Planing Boats," *Davidson Laboratory,* Nov. 1969

[3] Blount, Donald L. and Codega, Louis T. "Dynamic Stability of Planing Boats," *Marine Technology,* 29, (1992); 4-12

[4] Brown, Ward P. and Klosinski, Walter E. "Directional Stability Tests of Two Prismatic Planing Hulls," *Davidson Laboratory,* Jun. 1994

[5] Payne, Peter R. "Contributions to Planing Theory," *Ocean Engineering*, 7th ed. Vol 22, (1995); 699-729

[6] MacPherson, Donald M. "Sea trial analysis: The Value in the Data," *HydroComp Inc*, Jan. 2003

[7] van den Boom, H.J.J., Mennen, G.G.J., and Verkuyl J.B. "Sea Trial Analysis JIP: Recommended Practice for Speed Trials," Sep. 2006

[8] Bhawsinka, Karan, MEng Thesis, "Maneuvering simulation of displacement type ship and planing hull," Nov. 2011

[9] Sun, Hui and Faltinsen, Odd M "Dynamic motions of planing vessels in head seas," *Journal of Marine Science and Technology*, 2nd ed. Vol 16, (2011); 168-180

[10] American Bureau of Shipping "Guide for Vessel Maneuverability," Mar. 2006

[11] Petersen, Jóan Petur and Winther, Ole "Mining of Ship Operation Data for Energy Conservation," Jan. 2011

[12] Simon, Donald L. and Litt, Jonathan "A Data Filter for Identifying Steady-State Operating Points in Engine Flight Data for Condition Monitoring Applications," *Journal of Engineering for Gas Turbines and Power*, Vol 133, (2010)

[13] Trodden D.G., Murphy A.J., Pazouki, K., and Sargeant James "Fuel usage data analysis for efficient shipping operations," *Ocean Engineering*, Vol. 110, (2015); 75-84

[14] Zodiac Hurricane Technologies Inc "CCG SOLAS-H753; Stability Report," May 2015

[15] Mercury Cracing "Mercury NMEA 2000 Gateway," Jan. 2017

[16] Marine Traffic "Vessel details for: ROBERTS SISTERS II (Fishing Vessel) - IMO 8975433, MMSI 316010070, Call Sign Registered in Canada | AIS Marine Traffic," *Marine Traffic*, Jan. 2017 <https://www.marinetraffic.com/en/ais/details/ships/316010070>

[17] Fritsch, F. N. and Carlson, R. E. “Monotone piecewise cubic interpolation,” *SIAM Journal on Numerical Analysis*, 2nd ed. Vol 17, (1980); 238-246

[18] Mathworks “atan2,” Jan. 2017 <https://www.mathworks.com/help/matlab/ref/atan2.html>

[19] Mathworks “distance,” Jan. 2017 <https://www.mathworks.com/help/map/ref/distance.html>

[20] Savitsky, D. “Overview of planing hull developments,” *Proceedings of intersociety high performance marine vehicles conference*, Arlington, TX, Oct. 1992

Appendix A

Wave Buoy Specifications

Figure A.1: Bob

Figure A.2: Baby Bob

Appendix B

Turning Circle GPS Plots

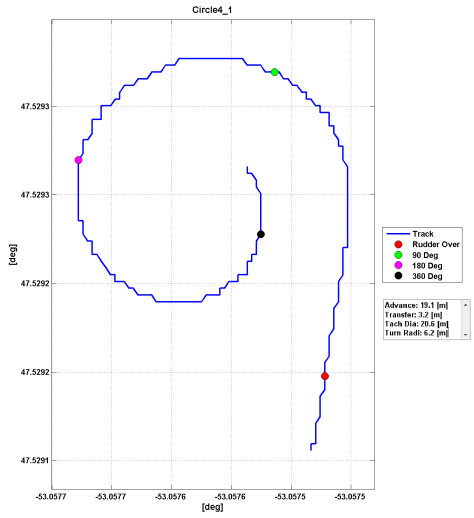

Figure B.1: Turning Circle 1 - 4 knots

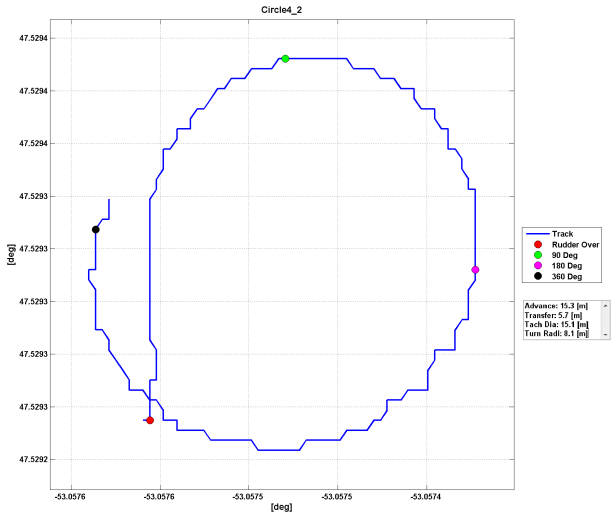

Figure B.2: Turning Circle 2 - 4 knots

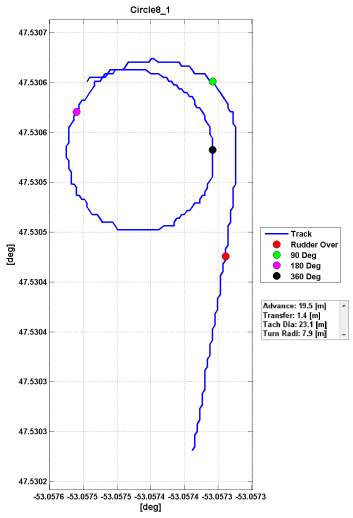

Figure B.3: Turning Circle - 8 knots

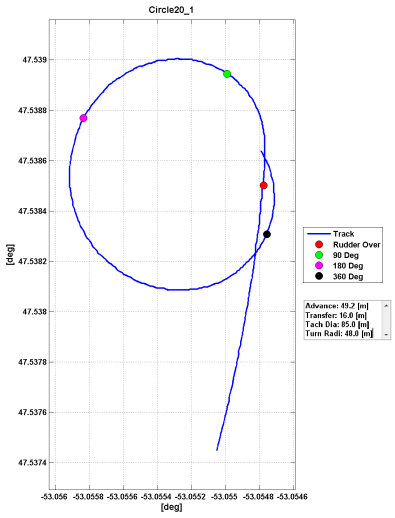

Figure B.4: Turning Circle 1 - 20 knots

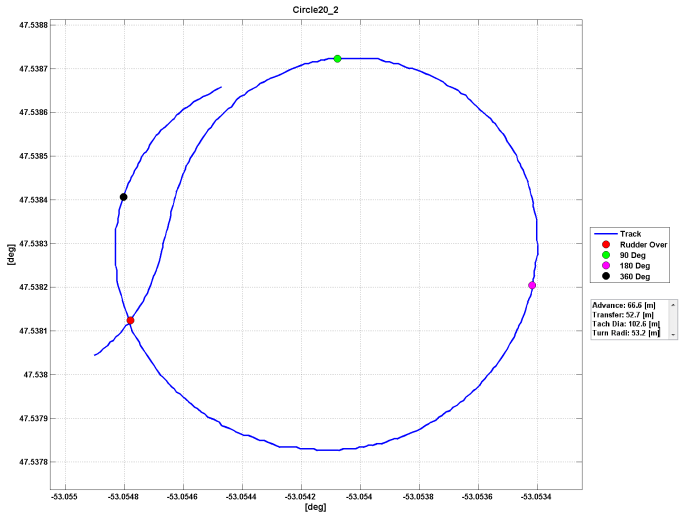

Figure B.5: Turning Circle 2 - 20 knots

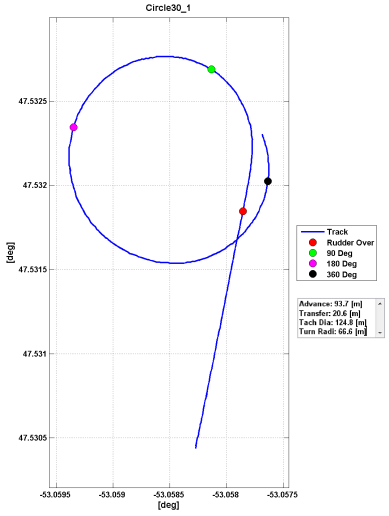

Figure B.6: Turning Circle 1 - 30 knots

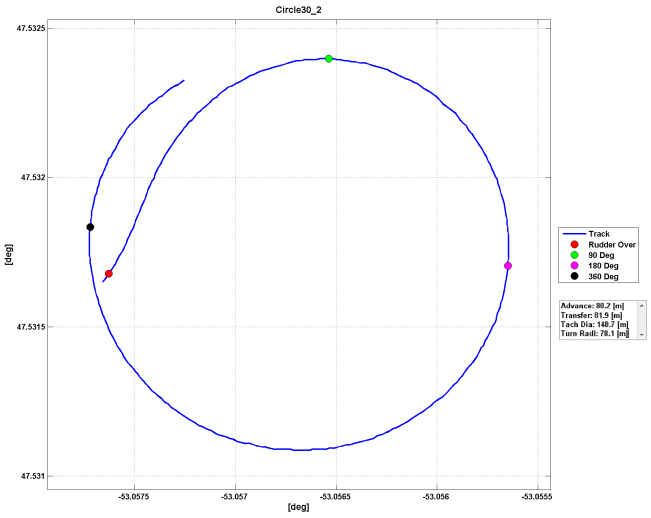

Figure B.7: Turning Circle 2 - 30 knots

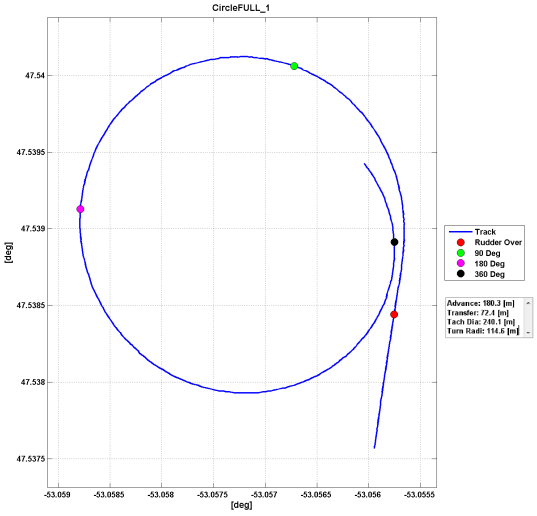

Figure B.8: Turning Circle 1 - 38 knots

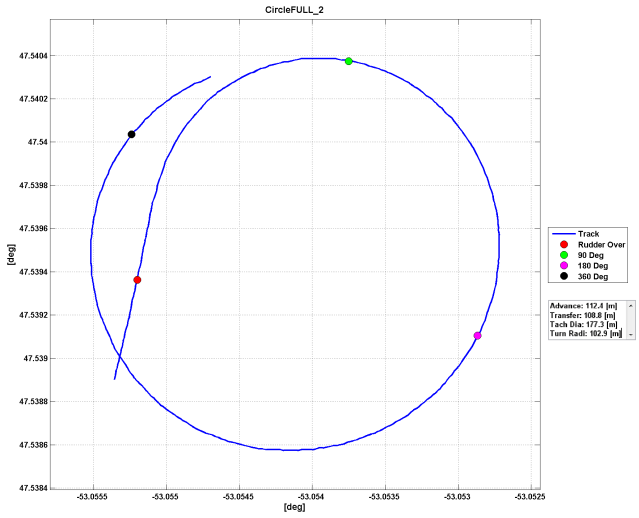

Figure B.9: Turning Circle 2 - 38 knots

Appendix C

Zig-zag GPS Plots

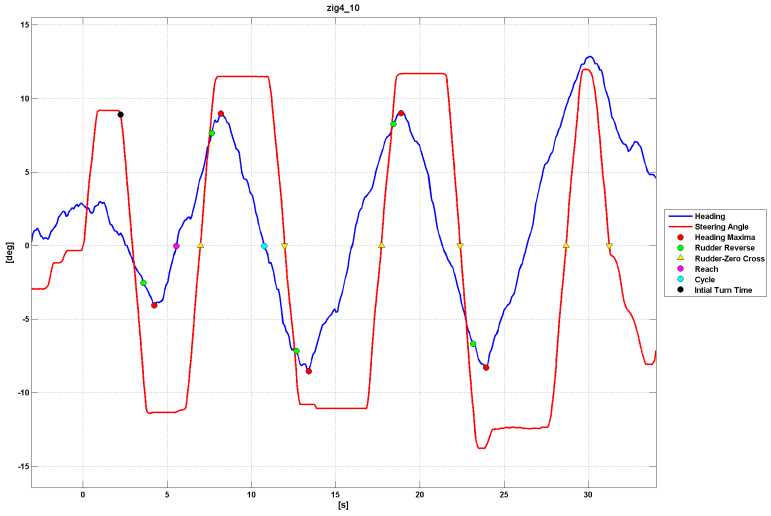

Figure C.1: Zig-zag - 4 knots - 10 degrees

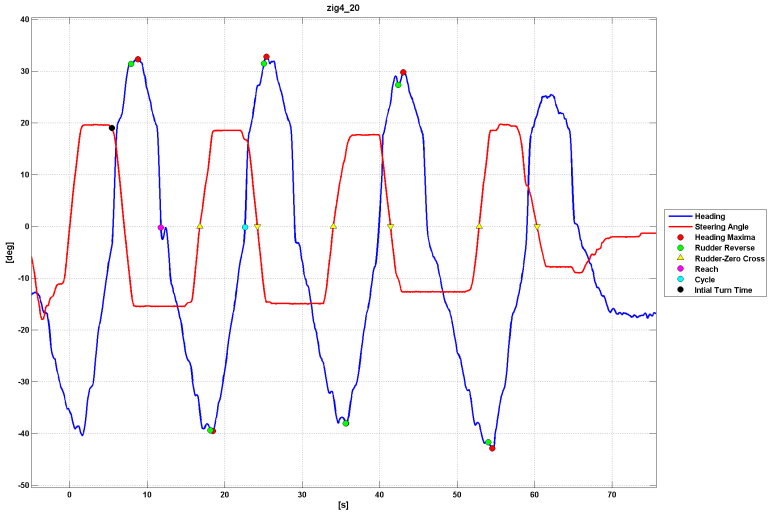

Figure C.2: Zig-zag - 4 knots - 20 degrees

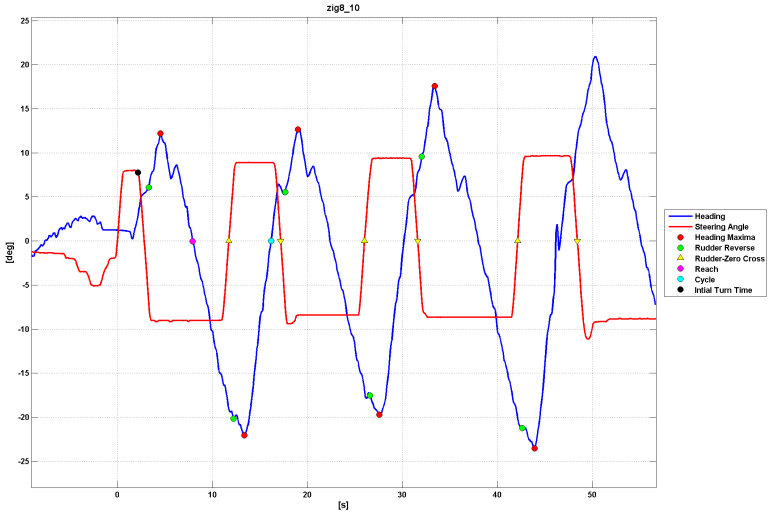

Figure C.3: Zig-zag - 8 knots - 10 degrees

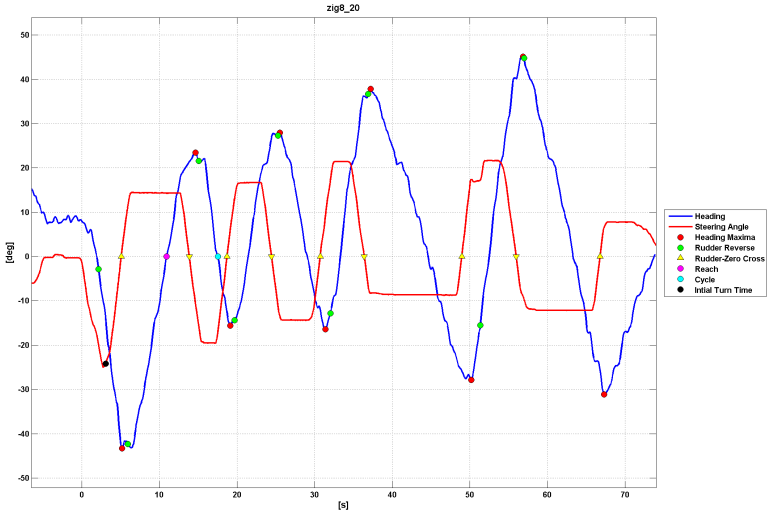

Figure C.4: Zig-zag - 8 knots - 20 degrees

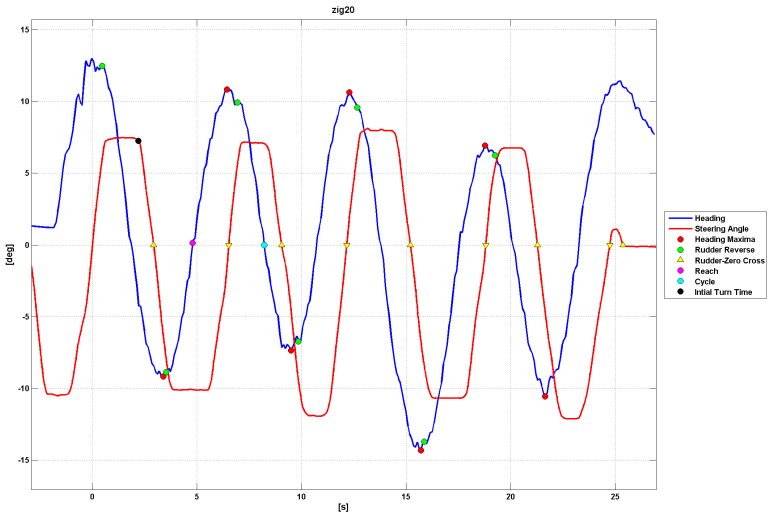

Figure C.5: Zig-zag - 20 knots - 10 degrees

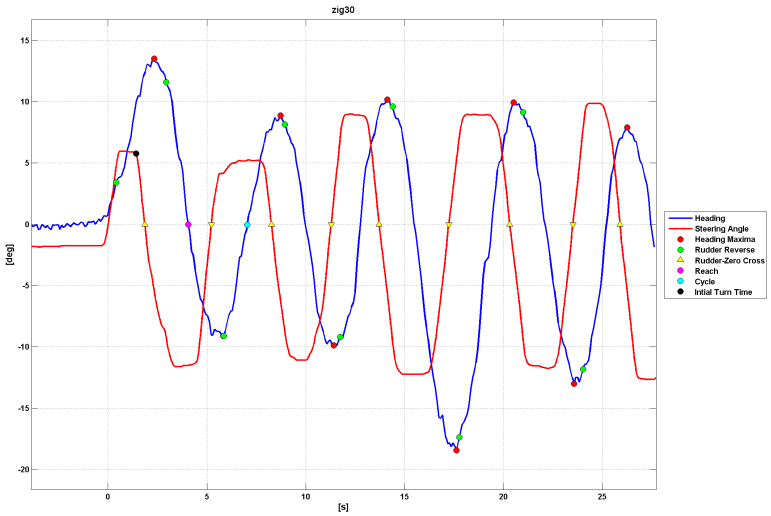

Figure C.6: Zig-zag - 30 knots - 10 degrees

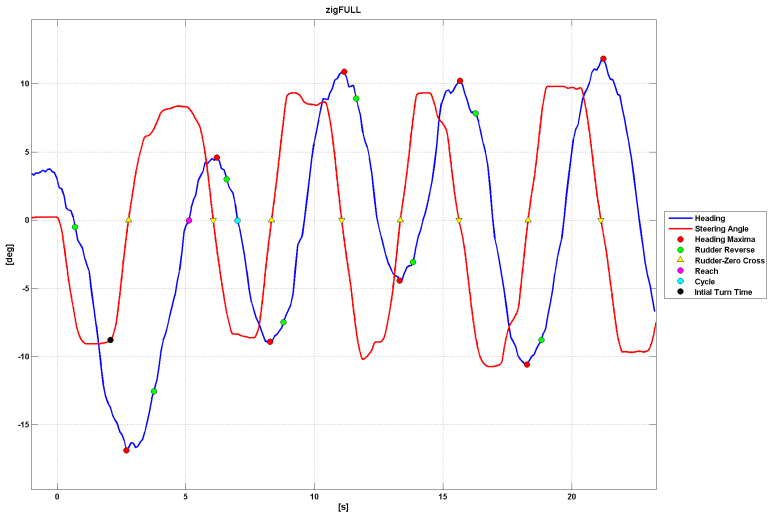

Figure C.7: Zig-zag - 38 knots - 10 degrees